Tria and quad plate finite elements based on RZT (m) for the analysis of multilayered sandwich structures

Tria and Quad plate finite elements based on RZT$^{(m)}$ for the analysis of multilayered sandwich structures

Marco Gherlone

Department of Mechanical and Aerospace Engineering
Politecnico di Torino
Corso Duca degli Abruzzi 24, 10129, Torino, Italy
Tel.: +390110906817
Fax: +390110906999
Email: marco.gherlone@polito.it

ABSTRACT

Aim of the paper is to develop and to assess a class of plate finite elements for the analysis of multilayered composite and sandwich structures. The adopted model is the mixed Refined Zigzag Theory (RZT$^{(m)}$), based on the kinematics of the Refined Zigzag Theory (RZT) and on the assumption of transverse shear stresses coming from integration of indefinite equilibrium equations. A triangular and quadrilateral flat finite element are developed by means of the Reissner's Mixed Variational Theorem and an interpolation strategy to eliminate shear locking. Several numerical examples are discussed to demonstrate the accuracy of RZT$^{(m)}$ and related finite elements for static response, free-vibrations and critical load problems of sandwich structures.

KEYWORDS

Sandwich plate; Refined Zigzag Theory; Reissner's Mixed Variational Theorem; Plate finite element

1. INTRODUCTION

A large number of papers dedicated to the analysis of multilayered composite and sandwich structures are available in the open literature because of the continuously increasing number of applications to aerospace, marine and civil engineering structures. Since their first appearance, multilayered beams, plates and shells have introduced several modeling issues not relevant to the study of isotropic and single-layer structures, i.e. transverse shear and normal deformability, transverse anisotropy, sensitivity to interlaminar damage.

Many of the existing approaches to multilayered structure analysis are based on the assumption of a through-the-thickness distribution of displacements, derivation of strains and stresses and application of the Principle of Virtual Works to obtain governing equations and consistent boundary conditions. The Equivalent Single-layer Theories (ESL) assume a through-the-thickness distribution of the displacement field along the entire laminate thickness. Increasing model complexity, from the Classical Lamination Plate Theory (CLPT) [1] and the First-order Shear Deformation Theory (FSDT) [2,3] to the higher-order theories [4,5], involves increasingly accurate transverse deformability, but the required continuity of transverse shear and normal stresses (computed from constitutive equations) cannot be met. According to Layer-Wise (LW) theories [6,7], through-the-thickness distribution of displacements is assumed for each layer and it is therefore possible to satisfy the continuity of transverse stresses. However, the number of unknowns of LW theories increase with the number of layers, leading to high computational costs, especially for complex structures and non-linear analyses. A compromise between low computational effort of ESL theories and accuracy of LW theories is represented by the zigzag theories involving a number of

kinematic unknowns which are not dependent on the number of layers and providing through-the-thickness continuous transverse shear stresses from the constitutive equations. Several zigzag theories have been presented, from the pioneering works of Di Sciuva [8,9] and Cho [10] to the recently proposed Refined Zigzag Theory (RZT) [11,12] (for a complete review of developed zigzag theories, refer to [13-15]). RZT has been proposed to address some drawbacks of the classic zigzag approaches (vanishing of transverse shear stresses at clamped boundaries and C^1-continuous shape functions for finite elements development [11]). The theory has seven kinematic variables (those of FSDT and two additional rotations related to zigzag kinematics) and relaxes the continuity condition on transverse shear stresses, which are piecewise constant. RZT has shown to be accurate over a wide range of stacking sequences and materials (ranging from single-layer [16] to multilayered composite and sandwich plates [17], including functionally graded materials [18]). Moreover, transverse shear stresses from constitutive equations provide an estimate of the layer-average value in most cases.

Another class of theories for multilayered structures are based on the Reissner's Mixed Variational Theorem (RMVT) [19] and on a through-the-thickness assumption for both displacements and transverse stresses. The latter are a-priori assumed to satisfy interlaminar continuity. From the first works of Murakami (ESL theory [20] and LW theory [21]), several other mixed approaches have been presented [22-26] (for a survey on existing mixed theories based on RMVT, see [27]). A key aspect of RMVT-based theories is the way transverse stresses are assumed a-priori. One possibility is to assume a totally independent transverse stress field, for example by expressing its through-the-thickness distribution as a polynomial expansion (typically piecewise parabolic [20]). This approach can run into some difficulty [28]. On the other hand, the through-the-

thickness shape of transverse stresses can be aided by using indefinite equilibrium equations [28], thus usually achieving higher degrees of accuracy.

An appealing combination can be obtained by using the RZT kinematic assumptions in the framework of a mixed approach where assumed transverse stresses are "inspired" by the use of indefinite equilibrium equations. Tessler has proposed the mixed Refined Zigzag Theory ($RZT^{(m)}$) for beams [29] and the relative beam finite elements [30]. Iurlaro *et al*. have extended $RZT^{(m)}$ to the plate case [31], where issues arising from an independent assumption of transverse stresses are investigated and confirmed.

Aim of the present paper is to formulate efficient triangular and quadrilateral finite elements based on $RZT^{(m)}$ for the analysis of multilayered structures. The basic assumptions and equations of $RZT^{(m)}$ for plates are summarized in Section 2. Plate finite elements are developed on the basis of C^0-continuous shape functions in Section 3. Numerical applications regarding sandwich structures in Section 4 assess the accuracy of both $RZT^{(m)}$ and related plate finite elements. This work is an extended version of [32].

2. MIXED REFINED ZIGZAG THEORY - $RZT^{(m)}$

In this section, the basic assumptions and fundamental definitions of $RZT^{(m)}$ for laminated composite and sandwich plates are reviewed to set the framework for the development of plate finite elements. For a complete treatment of RZT and $RZT^{(m)}$ for plates, refer to [12] and [31] respectively.

We consider a plate made of N perfectly bonded orthotropic layers referred to a Cartesian coordinate system (x_1, x_2, z), where $z \in [-h, +h]$ is the thickness coordinate and (x_1, x_2) map the in-plane domain (Figure 1).

FIGURE 1

Figure 1. Geometry of a plate and kinematic variables of the RZT$^{(m)}$.

The displacement field of RZT$^{(m)}$ taken from that of RZT can be written as

$$\begin{aligned} u_1^{(k)}(x_1, x_2, z, t) &= u(x_1, x_2, t) + z\theta_1(x_1, x_2, t) + \phi_1^{(k)}(z)\psi_1(x_1, x_2, t) \\ u_2^{(k)}(x_1, x_2, z, t) &= v(x_1, x_2, t) + z\theta_2(x_1, x_2, t) + \phi_2^{(k)}(z)\psi_2(x_1, x_2, t) \\ u_z(x_1, x_2, z, t) &= w(x_1, x_2, t) \end{aligned} \tag{1}$$

where superscript (k) denotes the association of a particular quantity to layer k^{th}. $u_1^{(k)}, u_2^{(k)}, u_z$ are the components of the displacement vector along axes (x_1, x_2, z) respectively, and depend on seven kinematic variables. Transverse displacement u_z is assumed to be constant through-the-thickness, simply represented by the deflection kinematic variable w. In-plane displacements exhibit a more complex distribution along the $z-$coordinate due to transverse anisotropy of multilayered composite and sandwich structures. Six kinematic variables are introduced representing uniform in-plane displacements (u, v), average bending rotations (θ_1, θ_2) and zigzag rotations (ψ_1, ψ_2). In particular, zigzag rotations measure the magnitude of the zigzag effect, i.e., distortion of the normal typical of layered structures. The through-the-thickness shape of this distortion is described by the zigzag functions $(\phi_1^{(k)}, \phi_2^{(k)})$ which depend on

thickness and transverse shear moduli of each layer (for detailed derivation of zigzag functions, see [12]).

Assuming linear strain-displacement relations, the strain components can be calculated as follows

$$\begin{aligned}
\varepsilon_{11}^{(k)} &= u_{,1} + z\theta_{1,1} + \phi_1^{(k)}\psi_{1,1} \\
\varepsilon_{22}^{(k)} &= v_{,2} + z\theta_{2,2} + \phi_2^{(k)}\psi_{2,2} \\
\gamma_{12}^{(k)} &= u_{,2} + v_{,1} + z\left(\theta_{1,2} + \theta_{2,1}\right) + \phi_1^{(k)}\psi_{1,2} + \phi_2^{(k)}\psi_{2,1} \\
\gamma_{1z}^{(k)} &= \gamma_1 + \beta_1^{(k)}\psi_1 \\
\gamma_{2z}^{(k)} &= \gamma_2 + \beta_2^{(k)}\psi_2
\end{aligned} \tag{2}$$

where $\gamma_\alpha \equiv w_{,\alpha} + \theta_\alpha$ and $\beta_\alpha^{(k)} \equiv \phi_{\alpha,z}^{(k)}$ (α=1,2). In-plane and transverse shear strains can be collected in vectors $\boldsymbol{\varepsilon} \equiv \left[\varepsilon_{11}^{(k)} \quad \varepsilon_{22}^{(k)} \quad \gamma_{12}^{(k)}\right]^T$ and $\boldsymbol{\gamma} \equiv \left[\gamma_{1z}^{(k)} \quad \gamma_{2z}^{(k)}\right]^T$ respectively. The corresponding stress components $\boldsymbol{\sigma} \equiv \left[\sigma_{11}^{(k)} \quad \sigma_{22}^{(k)} \quad \tau_{12}^{(k)}\right]^T$ and $\boldsymbol{\tau} \equiv \left[\tau_{1z}^{(k)} \quad \tau_{2z}^{(k)}\right]^T$, can be calculated using the well-known constitutive equations

$$\begin{aligned}
\boldsymbol{\sigma} &= \mathbf{C}\boldsymbol{\varepsilon} \\
\boldsymbol{\tau} &= \mathbf{Q}\boldsymbol{\gamma}
\end{aligned} \tag{3}$$

where $\mathbf{C} \equiv [C_{ij}^{(k)}]$ $(i, j = 1, 2, 6)$ and $\mathbf{Q} \equiv [Q_{\alpha\beta}^{(k)}]$ $(\alpha, \beta = 1, 2)$ are the matrices of transformed elastic stiffness coefficients referred to the (x_1, x_2, z) coordinate system, and based on the assumption that the transverse normal stress, σ_{zz}, can be neglected with respect to the in-plane stresses.

The governing equations of RZT$^{(m)}$ are derived using Reissner's Mixed Variational Theorem (RMVT) [19], here written assuming $\sigma_{zz} = 0$

$$\int_V \left(\delta \boldsymbol{\varepsilon}^T \boldsymbol{\sigma} + \delta \boldsymbol{\gamma}^T \hat{\boldsymbol{\tau}} + \delta \hat{\boldsymbol{\tau}}^T \left(\boldsymbol{\gamma} - \hat{\boldsymbol{\gamma}} \right) \right) dV - \delta W_e - \delta W_i = 0 \tag{4}$$

In Eq. (4), V is the volume of the plate, W_e is the work of external loads, W_i is the work of inertial loads, $\hat{\boldsymbol{\tau}} \equiv \left[\hat{\tau}_{1z}^{(k)} \quad \hat{\tau}_{2z}^{(k)} \right]^T$ is the vector of assumed transverse shear stresses and $\hat{\boldsymbol{\gamma}} \equiv \left[\hat{\gamma}_{1z}^{(k)} \quad \hat{\gamma}_{2z}^{(k)} \right]^T$ is the vector of the corresponding transverse shear strains

$$\hat{\boldsymbol{\tau}} = \mathbf{Q} \hat{\boldsymbol{\gamma}} \tag{5}$$

In the spirit of RMVT, $\hat{\boldsymbol{\tau}}$ are built in order (1) to constitute an equilibrated system with in-plane stresses, $\boldsymbol{\sigma}$, (2) to be through-the-thickness continuous and (3) to satisfy the traction equilibrium conditions on the external surfaces of the laminate

$$\left. \begin{array}{l} \tilde{\tau}_{\alpha z}^{(1)}(z=-h) = -\overline{p}_\alpha^b \\ \tilde{\tau}_{\alpha z}^{(N)}(z=+h) = +\overline{p}_\alpha^t \end{array} \right\} \quad (\alpha=1,2) \tag{6}$$

where $\overline{p}_\alpha^b$ and $\overline{p}_\alpha^t$ $(\alpha=1,2)$ are the surface-distributed tangential loads on the bottom and top surface of the laminate respectively. A convenient way to derive $\hat{\boldsymbol{\tau}}$ is to invoke the in-plane indefinite equilibrium equations (disregarding body forces)

$$\sigma_{\alpha\alpha,\alpha}^{(k)} + \tau_{\alpha\beta,\beta}^{(k)} + \hat{\tau}_{\alpha z,z}^{(k)} = 0 \quad (\alpha, \beta=1,2;\ \beta \neq \alpha) \tag{7}$$

Using the first of Eq. (6), Eq. (7) yields

$$\hat{\tau}_{\alpha z}^{(k)}(z) = -\overline{p}_{\alpha}^{b} - \int_{-h}^{z}\left(\sigma_{\alpha\alpha,\alpha}^{(k)} + \tau_{\alpha\beta,\beta}^{(k)}\right)dz \quad (\alpha,\beta=1,2;\ \beta\neq\alpha) \tag{8}$$

Substituting Eqs. (3) and (2) into Eq. (8) and then proceeding with mathematical manipulations provide expressions for $\hat{\tau}_{1z}^{(k)}$ and $\hat{\tau}_{2z}^{(k)}$ that depend on the eighteen second-order spatial derivatives of the RZT$^{(m)}$ in-plane kinematic variables $(u, v, \theta_1, \theta_2, \psi_1, \psi_2)$. This can lead to inaccuracy and over-fitting problems [28,31]. Therefore, the cylindrical bending assumption is made in the two planes (x_1, z) and (x_2, z), yielding a simplified expression for assumed transverse shear stresses [31]

$$\begin{aligned}
\hat{\tau}_{1z}^{(k)}(z) &= -\overline{p}_{1}^{b} - \left(\int_{-h}^{z} C_{11}^{(k)}dz\right)u_{,11} - \left(\int_{-h}^{z} zC_{11}^{(k)}dz\right)\theta_{1,11} - \left(\int_{-h}^{z} \phi_1^{(k)}C_{11}^{(k)}dz\right)\psi_{1,11} \\
\hat{\tau}_{2z}^{(k)}(z) &= -\overline{p}_{2}^{b} - \left(\int_{-h}^{z} C_{22}^{(k)}dz\right)v_{,22} - \left(\int_{-h}^{z} zC_{22}^{(k)}dz\right)\theta_{2,22} - \left(\int_{-h}^{z} \phi_2^{(k)}C_{22}^{(k)}dz\right)\psi_{2,22}
\end{aligned} \tag{9}$$

Enforcing satisfaction of second Eq. (6) enables us to eliminate $u_{,11}$ and $v_{,22}$ from Eqs. (9), thus obtaining [31]

$$\hat{\tau}_{\alpha z}^{(k)}(z) = Z_{\alpha}^{pb}(z)\cdot\overline{p}_{\alpha}^{b} + Z_{\alpha}^{pt}(z)\cdot\overline{p}_{\alpha}^{t} + Z_{\alpha}^{\theta}(z)\cdot\theta_{\alpha,\alpha\alpha} + Z_{\alpha}^{\psi}(z)\cdot\psi_{\alpha,\alpha\alpha} \quad (\alpha=1,2) \tag{10}$$

where $Z_{\alpha}^{pb}(z)$, $Z_{\alpha}^{pt}(z)$, $Z_{\alpha}^{\theta}(z)$ and $Z_{\alpha}^{\psi}(z)$ are function of the thickness coordinate, depend on the mechanical properties of the layers and guarantee that $\hat{\tau}_{1z}^{(k)}$ and $\hat{\tau}_{2z}^{(k)}$ stresses are through-the-thickness continuous and meet Eqs. (6) (refer to [31] for the definition of these functions). Following the procedure presented in [29], the second-order derivatives appearing in Eq. (10) are substituted by independent and unknown stress functions of in-plane coordinates, τ_{α}^{θ} and τ_{α}^{ψ} $(\alpha=1,2)$, thus obtaining

$$\hat{\tau}_{\alpha z}^{(k)}(z) = Z_{\alpha}^{pb}(z)\cdot \overline{p}_{\alpha}^{b} + Z_{\alpha}^{pt}(z)\cdot \overline{p}_{\alpha}^{t} + Z_{\alpha}^{\theta}(z)\cdot \tau_{\alpha}^{\theta} + Z_{\alpha}^{\psi}(z)\cdot \tau_{\alpha}^{\psi} \quad (\alpha=1,2) \tag{11}$$

As per Eq. (11), assumed transverse shear stresses $\hat{\boldsymbol{\tau}}$ are independent of the seven kinematic variables appearing in strain vectors $\boldsymbol{\varepsilon}$ and $\boldsymbol{\gamma}$. Therefore, variational statement (4) can be taken as the superposition of two independent statements

$$\begin{aligned} \int_V \left(\delta\hat{\boldsymbol{\tau}}^T\left(\boldsymbol{\gamma}-\hat{\boldsymbol{\gamma}}\right)\right)dV = 0 \\ \int_V \left(\delta\boldsymbol{\varepsilon}^T\boldsymbol{\sigma} + \delta\boldsymbol{\gamma}^T\hat{\boldsymbol{\tau}}\right)dV - \delta W_e - \delta W_i = 0 \end{aligned} \tag{12}$$

Using first Eq. (12), we express stress functions τ_{α}^{θ} and τ_{α}^{ψ} $(\alpha=1,2)$ in terms of transverse shear strain measures, γ_{α} and ψ_{α} $(\alpha=1,2)$, and of tangential loads $\overline{p}_{\alpha}^{b}$ and $\overline{p}_{\alpha}^{t}$ $(\alpha=1,2)$. A new expression for assumed transverse shear stresses is obtained

$$\hat{\tau}_{\alpha z}^{(k)}(z) = \tilde{Z}_{\alpha}^{pb}(z)\cdot \overline{p}_{\alpha}^{b} + \tilde{Z}_{\alpha}^{pt}(z)\cdot \overline{p}_{\alpha}^{t} + \tilde{Z}_{\alpha}^{\gamma}(z)\cdot \gamma_{\alpha} + \tilde{Z}_{\alpha}^{\psi}(z)\cdot \psi_{\alpha} \quad (\alpha=1,2) \tag{13}$$

Details of new through-the-thickness shape functions ($\tilde{Z}_{\alpha}^{pb}(z)$, $\tilde{Z}_{\alpha}^{pt}(z)$, $\tilde{Z}_{\alpha}^{\gamma}(z)$ and $\tilde{Z}_{\alpha}^{\psi}(z)$) can be found in [31]. The definition (13) of $\hat{\boldsymbol{\tau}}$ is then substituted, together with $\boldsymbol{\varepsilon}$, $\boldsymbol{\gamma}$ and $\boldsymbol{\sigma}$, into second Eq. (12), thus leading to the equations of motion and consistent boundary conditions of RZT$^{(m)}$ (refer to [31] for details).

3. PLATE FINITE ELEMENTS BASED ON RZT$^{(m)}$

This section presents the formulation of triangular ("tria") and quadrilateral ("quad") plate finite elements based on RZT$^{(m)}$.

It is simple to verify that first derivatives of the kinematic variables appear in the variational statement used to obtain the equilibrium equations of RZT$^{(m)}$ (second of Eqs. (12)). C^0-continuous shape functions are therefore necessary to formulate consistent finite elements. Shear-locking can occur, as was the case for RZT-based finite elements [33]. Adopting the original approach by Tessler and Dong [34] and the formulation of quadrilateral and triangular Mindlin plate finite elements [35,36] as well as RZT triangular finite elements [33], the anisoparametric interpolation is adopted to address and eliminate shear-locking. The deflection variable is interpolated using polynomials one-degree higher than those used for the bending and zigzag rotations. Consequently, nodal degrees of freedom are defined at corner nodes for all kinematic variables apart from the deflection requiring corresponding dofs also at the mid-edge nodes (Figure 2).

FIGURE 2

Figure 2. Topology of tria and quad finite elements based on anisoparametric interpolation.

For both the tria and the quad element, the interpolation of the kinematic variables can be written as follows

$$
\begin{aligned}
&u(x_1,x_2)=\sum_i u_i L_i(x_1,x_2), \quad v(x_1,x_2)=\sum_i v_i L_i(x_1,x_2)\\
&w(x_1,x_2)=\sum_\ell w_\ell P_\ell(x_1,x_2)\\
&\theta_\alpha(x_1,x_2)=\sum_i \theta_{\alpha i} L_i(x_1,x_2) \quad (\alpha=1,2)\\
&\psi_\alpha(x_1,x_2)=\sum_i \psi_{\alpha i} L_i(x_1,x_2) \quad (\alpha=1,2)
\end{aligned}
\tag{14}
$$

where $i = 1, 2, ..., n$ ranges over the n corner nodes ($n = 3$ for tria elements, $n = 4$ for quad elements), $\ell = 1, m_{12}, 2, m_{23}, ..., n, m_{n1}$ ranges over the corner and the mid-edge nodes. Moreover, L_i are the area-parametric coordinates for tria element and the isoparametric bi-linear shape functions for quad element [37]. Similarly, P_ℓ represent the quadratic shape functions for tria element and serendipity quadratic shape functions for quad element [37] (refer also to the Appendix). In other words, interpolation is isoparametric for all kinematic variables apart from deflection.

The approximation scheme represented by Eqs. (14) eliminates shear locking but can be further modified to have a simplified element topology. In particular, mid-edge nodes can be eliminated and the corresponding deflection dofs condensed out (see Figure 3) by adopting an edge-constraint strategy [33,35,36].

FIGURE 3

Figure 3. Simplified topology of constrained tria and quad finite elements based on anisoparametric interpolation.

Considering any edge of the tria and quad elements shown in Figure 2 (e.g. edge 12 as in Figure 4), it is possible to define a local coordinate *s* (parallel to the edge) as well as the components of bending and zigzag rotations normal to the edge (θ_n and ψ_n, easily written in terms of corresponding rotations of corner nodes).

FIGURE 4

Figure 4. Definition of edge quantities involved in constraint conditions.

It is subsequently possible to define two transverse shear strain measures [33]

$$\begin{aligned} \gamma_{sz} &\equiv w_{,s} + \theta_n \\ \eta_{sz} &\equiv \gamma_{sz} - \psi_n \end{aligned} \tag{15}$$

and simultaneously, two alternative edge constraining conditions

$$\begin{aligned} \frac{\partial \gamma_{sz}}{\partial s} &= 0 \\ \frac{\partial \eta_{sz}}{\partial s} &= 0 \end{aligned} \tag{16}$$

By enforcing the first or the second of Eqs. (16), the mid-edge node deflection can be expressed in terms of deflections, bending and zigzag rotations of the corresponding corner nodes. By applying the same constraint to all element edges, a new approximation is obtained for the deflection variable (in place of the second of Eqs. (14))

$$w(x_1, x_2) = \sum_i w_i L_i(x_1, x_2) + \sum_i \left(\left(\theta_{1i} + c\psi_{1i} \right) Q_{1i}(x_1, x_2) + \left(\theta_{2i} + c\psi_{2i} \right) Q_{2i}(x_1, x_2) \right) \tag{17}$$

where Q_{1i} and Q_{2i} are particular shape functions (see Appendix) and c is a flag parameter assuming two possible values:

- $c = 0$: γ_{sz} constant along each element edge;
- $c = -1$: η_{sz} constant along each element edge.

Substituting the approximation of deflection (Eq. (17)) and of the other kinematic variables (Eqs. (14)) into the definition of strain vectors $\boldsymbol{\varepsilon}$ and $\boldsymbol{\gamma}$ (Eqs. (2)) and of

stress vectors $\boldsymbol{\sigma}$ and $\hat{\boldsymbol{\tau}}$ (the first of Eqs. (3) and Eq. (13)) and applying the variational statement (second of Eqs. (12)) leads to the discretized equations of motion for RZT$^{(m)}$ tria and quad finite elements and to the definition of the related stiffness and mass matrices. Similarly, it is possible to obtain the geometric stiffness matrix for linear buckling analyses.

4. NUMERICAL RESULTS

Firstly, a set of numerical results is presented in order to review RZT$^{(m)}$ performance versus that of RZT for the static response analysis of sandwich structures under different loading and boundary conditions. Subsequently, the accuracy and convergence of RZT$^{(m)}$-based plate finite elements is investigated for static response, free vibrations and buckling analysis of sandwich plates.

4.1 Geometry and material properties

Rectangular plates sized a x b and total thickness $2h$ are analyzed. Sandwich stacking sequences (both symmetric and non-symmetric) having a polymeric foam core and metallic or multilayered composite facesheets are considered (Table 1). For material mechanical properties, see Table 2. Laminate IA* is based on the same properties of laminate IA but with varying core mechanical properties R*, i.e. Young and shear moduli of core material R are multiplied by variable coefficient λ).

Table 1. Stacking sequences of the considered laminates (layer sequence is in positive *z*-direction).

Laminate code	Thicknesses ($h^{(k)}/h$)	Materials	Orientations (degrees)
IS	($\frac{1}{10}$ / $\frac{8}{10}$ / $\frac{1}{10}$)	(A/R/A)	(0/0/0)
IA	($\frac{1}{10}$ / $\frac{7}{10}$ / $\frac{2}{10}$)	(A/R/S)	(0/0/0)
IA*	($\frac{1}{10}$ / $\frac{7}{10}$ / $\frac{2}{10}$)	(A/R*/S)	(0/0/0)
CS	($\frac{1}{30}$ / $\frac{1}{30}$ / $\frac{1}{30}$ / $\frac{24}{30}$ / $\frac{1}{30}$ / $\frac{1}{30}$ / $\frac{1}{30}$)	(C/C/C/R/C/C/C)	(0/90/0/0/90/0/90)
CA	($\frac{1}{30}$ / $\frac{1}{30}$ / $\frac{1}{30}$ / $\frac{21}{30}$ / $\frac{2}{30}$ / $\frac{2}{30}$ / $\frac{2}{30}$)	(C/C/C/R/C/C/C)	(0/90/0/0/0/90/0)

Table 2. Material mechanical properties.

Material code	E_1 (MPa)	E_2 (MPa)	E_3 (MPa)	ν_{12}	ν_{13}	ν_{23}	G_{12} (MPa)	G_{13} (MPa)	G_{23} (MPa)
C (Carbon-Epoxy UD)	110000	7857	7857	0.33	0.33	0.49	3292	3292	1292
R (Rohacell® foam)	40.3			0.3			12.4		
R* (Rohacell® foam of variable stiffness according to λ)	40.3 λ			0.3			12.4 λ		
A (Aluminum alloy)	73000			0.3					
S (Steel)	210000			0.3					

Where applicable, results are presented in non-dimensional form according to the following definitions

$$\left.\begin{aligned} \left(\tilde{u}_\alpha, \tilde{w}\right) &\equiv \left(u_\alpha, w\right)\cdot\left(\frac{D_{11}}{q_0 a^4}\right) \\ \tilde{\sigma}_{\alpha\alpha} &\equiv \sigma_{\alpha\alpha}\cdot\left(\frac{1}{q_0}\left(\frac{2h}{a}\right)^2\right) \\ \tilde{\tau}_{\alpha z} &\equiv \tau_{\alpha z}\cdot\left(\frac{1}{q_0}\left(\frac{2h}{a}\right)\right) \end{aligned}\right\} \quad (\alpha=1,2) \tag{18}$$

where q_0 is the magnitude of applied transverse distributed load, D_{11} is the bending stiffness of the plate along the x_1-axis and $\tau_{\alpha z}$ represent assumed transverse shear stresses for RZT$^{(m)}$ ($\hat{\boldsymbol{\tau}}$) and transverse shear stresses coming from constitutive equations for RZT.

4.2 Assessment of RZT$^{(m)}$ performance

To appreciate the benefits of the RZT$^{(m)}$ mixed approach, especially in terms of through-the-thickness distribution of transverse shear stresses, simply supported square plates ($a = b$) subjected to bi-sinusoidal transverse load $q(x_1, x_2) = q_0 \sin(\pi x_1 / a)\sin(\pi x_2 / b)$ are considered. The plates selected are moderately thick, $a/2h = 10$. For both RZT and RZT$^{(m)}$, the exact Navier-type solution for equilibrium equations is obtained using trigonometric expressions of in-plane coordinates for the kinematic variables

$$\begin{aligned} w &= W \sin(\pi x_1 / a)\sin(\pi x_2 / b) \\ \{u, \theta_1, \psi_1\} &= \{U, \Theta_1, \Psi_1\} \cos(\pi x_1 / a)\sin(\pi x_2 / b) \\ \{v, \theta_2, \psi_2\} &= \{V, \Theta_2, \Psi_2\} \sin(\pi x_1 / a)\cos(\pi x_2 / b) \end{aligned} \tag{19}$$

Reference results considered are those provided by the exact elasticity solution [38].

Table 3 shows maximum non-dimensional deflection (at plate center, $x_1 = a/2$ and $x_2 = b/2$) for different stacking sequences.

Table 3. Maximum non-dimensional deflection, $\tilde{w}$.

Laminate code	Exact elasticity [38]	RZT	RZT$^{(m)}$
IS	1.106e-01	1.106e-01	1.106e-01
IA	1.044e-01	1.049e-01	1.050e-01
CS	9.369e-02	9.366e-02	9.368e-02
CA	1.200e-01	1.198e-01	1.201e-01

Both RZT and RZT$^{(m)}$ provide excellent response predictions in terms of maximum deflection for the challenging stacking sequences considered. The same level of accuracy is unachievable by the classical Equivalent Single Layer approaches such as CLPT and FSDT (even using ad-hoc shear correction factors), as shown in [17]. This level of performance is guaranteed to both RZT and RZT$^{(m)}$ by the common kinematic assumptions that, with a reduced number of kinematic variables (number-of-layers independent), are able to model the through-the-thickness normal distortion ("zigzag effect") typical of multilayered composite and sandwich structures. This conclusion is also supported by the analysis of the through-the-thickness distribution of in-plane displacements and stresses for laminate CA (Figures 5-7).

FIGURE 5

Figure 5. Laminate CA, simply supported square plate, sinusoidal transverse load: through-the-thickness distribution of non-dimensional in-plane displacement $\tilde{u}_1$.

FIGURE 6

Figure 6. Laminate CA, simply supported square plate, sinusoidal transverse load: through-the-thickness distribution of non-dimensional in-plane stress $\tilde{\sigma}_{11}$.

FIGURE 7

Figure 7. Laminate CA, simply supported square plate, sinusoidal transverse load: through-the-thickness distribution of non-dimensional in-plane stress $\tilde{\sigma}_{22}$.

Results obtained using RZT and RZT$^{(m)}$ are almost identical for in-plane displacements (Figure 5) and for in-plane axial stresses (Figures 6 and 7). Different levels of performance can be observed for transverse shear stresses (obtained from constitutive equations for RZT and assumed for RZT$^{(m)}$). See Figures 8 and 9 for laminate CA, Figures 10-12 for the other laminates.

FIGURE 8

Figure 8. Laminate CA, simply supported square plate, sinusoidal transverse load: through-the-thickness distribution of non-dimensional transverse shear stress $\tilde{\tau}_{1z}$.

FIGURE 9

Figure 9. Laminate CA, simply supported square plate, sinusoidal transverse load: through-the-thickness distribution of non-dimensional transverse shear stress $\tilde{\tau}_{2z}$.

FIGURE 10

Figure 10. Laminate CS, simply supported square plate, sinusoidal transverse load: through-the-thickness distribution of non-dimensional transverse shear stress $\tilde{\tau}_{1z}$.

FIGURE 11

Figure 11. Laminate IS, simply supported square plate, sinusoidal transverse load: through-the-thickness distribution of non-dimensional transverse shear stress $\tilde{\tau}_{1z}$.

FIGURE 12

Figure 12. Laminate IA, simply supported square plate, sinusoidal transverse load: through-the-thickness distribution of non-dimensional transverse shear stress $\tilde{\tau}_{1z}$.

RZT produces a piecewise constant distribution of transverse shear stresses that, in most cases, is able to provide an evaluation of the average stress at the layer level. This can be seen in Figure 11 for the core and both facesheets, and in Figure 12 for the core and top facesheet. These results were obtained for sandwich panels (IS and IA) with single-layered faces. When the stacking sequence is symmetric (laminate IS), results obtained with RZT are accurate (in an average sense), whereas when there is no symmetry (laminate IA), the average transverse shear stress can be underestimated or overestimated in one of the facesheets (as is the case for the bottom layer which is thinner and with a weaker material than in the top face). When faces are multilayered (laminates CA and CS, Figures 8-10), RZT can run into more evident difficulties in the facesheets. Adopting the classic procedure based on integrating the indefinite equilibrium equations, would help RZT to obtain much more accurate results in most cases [18,31]. However, this approach becomes less attractive in the framework of finite element solutions due to the need for higher-order polynomials as shape functions.

$RZT^{(m)}$ can model with high accuracy the through-the-thickness distribution of transverse shear stresses for all cases considered (Figures 8 through 12). The resulting curves are reliable and accurate in a point-wise sense and within all layers. This critical improvement of $RZT^{(m)}$ relative to RZT is obtained with no increase in computational cost (the same number of kinematic unknowns is used) and without using any post-processing procedure (integration of indefinite equilibrium equations).

4.3 Comparison of $RZT^{(m)}$ FEM constraining strategies

As explained in Section 3, two constraining strategies can be adopted to develop plate finite elements based on $RZT^{(m)}$ with a simplified topology (nodal degrees of

freedom defined only at corner nodes). To establish their relative merit, the performance of elements implemented must be compared for both strategies.

We reconsider a simply-supported, moderately thick square plate ($a = b$, $a/2h = 10$) subjected to a bi-sinusoidal transverse load $q(x_1, x_2) = q_0 \sin(\pi x_1 / a)\sin(\pi x_2 / b)$ with stacking sequence IA*. As a reference result, we use the RZT$^{(m)}$ analytical solution, i.e. the exact trigonometric solution of the equilibrium equations within the framework of RZT$^{(m)}$ (Eq. (19)). Different solutions are also obtained with RZT$^{(m)}$-based finite elements. Since the aim of this analysis is to assess only the available constraining strategies, a high-fidelity mesh is adopted to assure converging results. Taking advantage of problem symmetries, only ¼ of the plate is modeled, and a uniform mesh is used having 50 subdivisions of each plate half-edge. Thus, the number of elements used in ¼ of the plate is 2500 for quad elements and 5000 for tria elements, the number of nodes and nodal degrees of freedom being the same. Figure 13 shows an example of mesh patterns for quad and tria elements.

FIGURE 13

Figure 13. Mesh patterns for quad and tria elements on ¼ of the plate (dash-dotted lines represent symmetry axes). Both mesh schemes are denoted by 8 x 8, meaning the number of FEM subdivisions along each edge. The total number of elements is 64 for quad and 128 for tria. There are 81 nodes and 567 nodal degrees of freedom in both cases.

The percent error on the maximum deflection is

$$E_w \equiv 100\left(\frac{w_{\max}^{FEM} - w_{\max}^{ANA}}{w_{\max}^{ANA}} \right) \tag{20}$$

where "ANA" refers to the analytical solution and "FEM" to the finite element results. In order to consider the effect of stacking sequence on E_w, the core mechanical properties are allowed to change (material R*, Table 2) and a transverse anisotropy parameter is defined as follows

$$r \equiv \frac{E_C}{\left(\frac{E_{Ftop} + E_{Fbot}}{2} \right)} \tag{21}$$

where $E_C = 40.3\lambda$ (see Table 2) is the Young modulus of the core (different for any of the considered laminates), and E_{Fbot} and E_{Ftop} are the Young modulus of the bottom and top facesheet respectively (the same for all laminates). Figure 14 shows the effect of r on E_w for different element shapes (tria or quad, denoted by "T" and "Q" respectively) and different constraining strategies (based on γ_{sz} or on η_{sz}, denoted by superscript "γ" or and "η" respectively, see Eqs. (16)).

FIGURE 14

Figure 14. Laminate IA* (varying r), simply supported square plate, sinusoidal transverse load: percent error on maximum deflection E_w, as a function of transverse anisotropy ratio r, for different RZT$^{(m)}$-based finite elements and different constraining strategies (50 x 50 mesh on ¼ plate).

For stacking sequences exhibiting medium-to-low transverse anisotropy, $r \in (10^{-2}, 1)$, all element shapes and constraining strategies show accurate results. For highly transverse-anisotropic plates $r < 10^{-2}$, different performances are observed. Elements based on "η" constraining strategy are still accurate, whereas those based on

"γ" constraint lead to non-negligible errors (especially for tria elements). Elements based on "η" constraining strategy exhibit excellent response predictions over the whole interval of parameter r, ranging from highly heterogeneous laminates to scarcely anisotropic lay-ups. The investigation is extended to the through-the-thickness distribution of in-plane axial and transverse shear stresses for the highly heterogeneous case, $r = 10^{-5}$ (Figures 15-18, where "RZT$^{(m)}$" refers to the analytical solution). The through-the-thickness distributions are computed (for both FEM and analytical solution) at the centroid of a specific element shown in each Figure. Considering that the mesh is highly refined, the accuracy of this choice is deemed acceptable.

FIGURE 15

Figure 15. Laminate IA* ($r = 10^{-5}$), simply supported square plate, sinusoidal transverse load: through-the-thickness distribution of non-dimensional in-plane stress $\tilde{\sigma}_{11}$, using RZT$^{(m)}$-quad elements and different constraining strategies (50 x 50 mesh on ¼ plate). Maximum percent errors (FEM vs RZT$^{(m)}$) are –0.02% for Q^{η} and –2.50% for Q^{γ}.

FIGURE 16

Figure 16. Laminate IA* ($r = 10^{-5}$), simply supported square plate, sinusoidal transverse load: through-the-thickness distribution of non-dimensional in-plane stress $\tilde{\sigma}_{11}$, using RZT$^{(m)}$-tria elements and different constraining strategies (50 x 50 mesh on ¼ plate). Maximum percent errors (FEM vs RZT$^{(m)}$) are –0.02% for T^{η} and +2.76% for T^{γ}.

FIGURE 17

Figure 17. Laminate IA* ($r = 10^{-5}$), simply supported square plate, sinusoidal transverse load: through-the-thickness distribution of non-dimensional transverse shear stress $\tilde{\tau}_{1z}$, using RZT$^{(m)}$-quad elements and different constraining strategies (50 x 50 mesh on ¼ plate). Maximum percent errors (FEM vs RZT$^{(m)}$) are +1.86% for Q^{η} and +0.27% for Q^{γ}.

FIGURE 18

Figure 18. Laminate IA* ($r = 10^{-5}$), simply supported square plate, sinusoidal transverse load: through-the-thickness distribution of non-dimensional transverse shear stress $\tilde{\tau}_{1z}$, using RZT$^{(m)}$-tria elements and different constraining strategies (50 x 50 mesh on ¼ plate). Maximum percent errors (FEM vs RZT$^{(m)}$) are –0.80% for T^{η} and –14.42% for T^{γ}.

The performance of quad and tria elements for the evaluation of in-plane axial stresses is found to be the same (Figures 15 and 16). Using "η" elements results in less than 0.1% errors compared to the analytical solution, whereas "γ" constraint produces slightly larger errors (2.50% approx.). As regards transverse shear stresses, more pronounced differences are observed (Figures 17 and 18). "η" elements maintain high accuracy, whereas "γ" elements can become inaccurate, especially for tria elements. The superior predictive capabilities obtained using the constraining condition based on η_{sz} strain measure were previously confirmed for tria elements based on RZT [33] and are now confirmed for both tria and quad elements based on RZT$^{(m)}$.

4.4 Convergence analysis

Convergence properties of "η" elements are investigated extending the analyses from static response to free vibration and to buckling loads.

Initially, we consider two static problems, i.e. (1) a square plate (laminate CA) with two opposite clamped edges subjected to a uniformly distributed transverse load and (2) a simply supported square plate (laminate IA) under a sinusoidal transverse load. Both problems are solved considering only ¼ of the plate for reasons of symmetry, and adopting regular mesh schemes n_e x n_e (Figure 13). For reference results we use an analytical solution based on RZT$^{(m)}$, i.e. the usual Navier-type exact solution for

problem (2) and a Rayleigh-Ritz type solution for problem (1)[1]. Figures 19 and 20 show to what extent maximum deflection percent error (Eq. (20)) is influenced by the number of FEM subdivisions along each edge of ¼ plate, n_e.

FIGURE 19

Figure 19. Laminate CA, clamped-free-clamped-free square plate, uniform transverse load: percent error on maximum deflection E_w, as a function of number of T^η and Q^η subdivisions n_e, along each edge of ¼ plate.

FIGURE 20

Figure 20. Laminate IA, simply supported square plate, sinusoidal transverse load: percent error on maximum deflection E_w, as a function of number of T^η and Q^η subdivisions n_e, along each edge of ¼ plate.

For both problems, a 10 x 10 mesh assures an error E_w<1% for Q^η elements (slightly more accurate than T^η especially with fewer elements).

Subsequently, we consider two free-vibration problems: (1) a cantilevered square plate (laminate IA) and (2) a simply supported square plate (laminate CS). The finite element solution with mesh pattern n_e x n_e is applied to the whole plate. The analytical reference solutions are obtained using the Rayleigh-Ritz approach for problem (1)[2] and the Navier-type solution for problem (2). The accuracy of FEM results is established by evaluating the percent error of natural frequencies

$$E_\omega \equiv 100\left(\frac{\omega_i^{FEM} - \omega_i^{ANA}}{\omega_i^{ANA}}\right) \tag{22}$$

[1] All kinematic variables are approximated using Gram-Schmidt polynomials built with 11 functions along each of the coordinate axes [12].
[2] All kinematic variables are approximated using Gram-Schmidt polynomials built with 11 functions along x_1-axis and 7 functions of x_2-coordinate [12].

Figures 21 and 22 show the variation of E_ω with n_e for 1st and 5th mode.

FIGURE 21

Figure 21. Laminate IA, cantilevered square plate: percent error on 1st and 5th natural frequency E_ω, as a function of number of T^η and Q^η subdivisions n_e, along each plate edge.

FIGURE 22

Figure 22. Laminate CS, simply supported square plate: percent error on 1st and 5th natural frequency E_ω, as a function of number of T^η and Q^η subdivisions n_e, along each plate edge.

A 8 x 8 Q^η mesh ensures E_ω<5% up to the 5th mode for both problems, whereas 9 x 9 T^η elements are required to achieve the same accuracy for the cantilevered plate (Figure 21), i.e. Q^η are once again slightly more accurate than T^η.

Linear buckling analysis is performed on a simply supported plate (laminate CS) subjected to uniaxial in-plane load N distributed along two opposite edges. Two cases are considered: (1) square plate and (2) rectangular plate with a/b=1.7, loaded on short edges. A n_e x n_e mesh scheme is adopted for the square plate, whereas the rectangular plate is modeled with n_e subdivisions along short edges and $1.7n_e$ (rounded up) on long edges. The Navier-type solution is used to provide analytical reference results, and the percent error on the critical load is evaluated

$$E_N \equiv 100\left(\frac{N_{cr}^{FEM} - N_{cr}^{ANA}}{N_{cr}^{ANA}}\right) \tag{23}$$

Figures 23 and 24 show the changes in E_N with n_e for square and rectangular plate respectively.

FIGURE 23

Figure 23. Laminate IS, simply supported square plate: percent error on critical load E_N, as a function of number of T^η and Q^η subdivisions n_e, along each plate edge.

FIGURE 24

Figure 24. Laminate IS, simply supported rectangular plate: percent error on critical load E_N, as a function of number of T^η and Q^η subdivisions n_e, along short plate edges.

Q^η elements converge much faster than T^η elements. n_e=9 and n_e =8 with Q^η elements ensures E_N<5% for square and rectangular plate respectively. The same performance are achieved for T^η elements with n_e=12 and n_e =11.

5. CONCLUSIONS

The paper summarizes the basic properties of the mixed Refined Zigzag Theory ($RZT^{(m)}$) for plates. The kinematic assumptions, common to the Refined Zigzag Theory (RZT), include enhancing in-plane displacement field with through-the-thickness piecewise linear distributions that model the normal distortion typical of multilayered structures. Transverse shear stresses are assumed starting from the integration of in-plane indefinite equilibrium equations. The Reissner's Mixed Variational Theorem is then used to obtain governing equations and boundary conditions.

Triangular and quadrilateral C^0 finite elements based on $RZT^{(m)}$ are introduced for the first time. Anisoparametric interpolation is used to avoid shear locking and two alternative edge-constraint strategies are adopted to simplify elements' topology so as to have only corner nodes and related degrees of freedom.

A set of example problems are tested for static response, free vibrations and critical load of sandwich plates with metallic or multilayered composite facesheets and foam core. Initially, the enhanced modelling performances of RZT$^{(m)}$ compared to RZT are demonstrated, especially regarding through-the-thickness distribution of transverse shear stresses. Subsequently, the RZT$^{(m)}$-based finite elements, are tested showing that the constraining strategy based on "η" transverse shear strain measure is preferable, since it provides accurate results over a wide range of plate transverse anisotropy. Upon investigation, the performance of tria and quad elements indicates that the convergence rate for the quad element is slightly better.

The tria and quad RZT$^{(m)}$-based finite elements proposed and assessed prove accurate in different applications and computationally affordable. They are an effective numerical tool for analysis of multilayered composite and sandwich plates, hopefully finding implementation in FEM commercial codes. Moreover, the accuracy of through-the-thickness distribution of in-plane and transverse shear stresses (also for highly anisotropic lay-ups) indicates that RZT$^{(m)}$-based elements are appropriate for the analysis of multilayered structures exhibiting intra- and inter-laminar damage (as already shown for beam structures [30]).

A further natural extension of this research effort will be the development of shell finite elements for built-up and curved multilayered structure analysis.

APPENDIX

The definition of quadratic shape functions P_ℓ for triangular element [37], appearing in the initial approximation of deflection (Eqs. (14)) is

$$
\begin{aligned}
&P_i \equiv L_i\left(2L_i-1\right) \quad \left(i=1,2,3\right)\\
&P_{ij} \equiv 4L_iL_j \qquad \begin{pmatrix} i=1,2,3 \\ j=2,3,1 \end{pmatrix}
\end{aligned}
\tag{A1}
$$

where L_i are the area-parametric coordinates. For quadrilateral element, P_ℓ are the biquadratic serendipity shape functions [37]

$$
\begin{aligned}
&P_i \equiv \frac{1}{4}\left(1+\xi_i\xi\right)\left(1+\eta_i\eta\right)\left(\xi_i\xi+\eta_i\eta-1\right) \quad \left(i=1,2,3,4\right)\\
&P_{12} \equiv \frac{1}{2}\left(1-\xi^2\right)\left(1-\eta\right)\\
&P_{23} \equiv \frac{1}{2}\left(1-\eta^2\right)\left(1+\xi\right)\\
&P_{34} \equiv \frac{1}{2}\left(1-\xi^2\right)\left(1+\eta\right)\\
&P_{41} \equiv \frac{1}{2}\left(1-\eta^2\right)\left(1-\xi\right)
\end{aligned}
\tag{A2}
$$

where (ξ,η) are the element local in-plane coordinates, $(\xi,\eta)\in\left[-1,+1\right]$, and (ξ_i,η_i) are the local coordinates of corner node i^{th}.

Shape functions Q_{1i} and Q_{2i} appearing in the final, "constrained" approximation of deflection (Eq. (17)) are defined as

$$
\left.\begin{aligned}
Q_{1i} &\equiv \frac{L_i}{2}\left[L_j\left(x_{1i}-x_{1j}\right)+L_k\left(x_{1i}-x_{1k}\right)\right]\\
Q_{2i} &\equiv \frac{L_i}{2}\left[L_j\left(x_{2i}-x_{2j}\right)+L_k\left(x_{2i}-x_{2k}\right)\right]
\end{aligned}\right\} \quad \begin{pmatrix} i=1,2,3 \\ j=2,3,1 \\ k=3,1,2 \end{pmatrix}
\tag{A3}
$$

for the triangular element, and as

$$\left.\begin{aligned} Q_{1i} &\equiv \frac{1}{8}\left[P_{ki}\left(x_{1i}-x_{1k}\right)+P_{ij}\left(x_{1i}-x_{1j}\right)\right] \\ Q_{2i} &\equiv \frac{1}{8}\left[P_{ki}\left(x_{2i}-x_{2k}\right)+P_{ij}\left(x_{2i}-x_{2j}\right)\right] \end{aligned}\right\} \quad \begin{pmatrix} i=1,2,3,4 \\ j=2,3,4,1 \\ k=4,1,2,3 \end{pmatrix} \tag{A4}$$

for the quadrilateral element, where (x_{1i}, x_{2i}) are the coordinates of node i^{th} and functions P_{ki} and P_{ij} are as defined in Eq. (A2).

REFERENCES

[1] Reissner, E., Stavsky, Y., 1961, "Bending and stretching of certain types of heterogeneous aeolotropic elastic plates", Journal of Applied Mechanics, 28(3), pp. 402 – 408.

[2] Reissner, E., 1945, "The effect of transverse shear deformation on the bending of elastic plates", Journal of Applied Mechanics, 12, pp. 68 – 77.

[3] Mindlin, R.D., 1951, "Influence of rotatory inertia and shear deformation on flexural motions of isotropic elastic plates", Journal of Applied Mechanics, 18, pp. 31 – 38.

[4] Reddy, J.N., 1984, "A simple higher-order theory for laminated composite plates", Journal of Applied Mechanics, 51(4), pp. 745 – 752.

[5] Touratier, M., 1991, "An efficient standard plate theory", International Journal of Engineering Science, 29, pp. 901 – 916.

[6] Reddy, J.N., 1987, "A generalization of two-dimensional theories of laminated composite plates", Communications in Applied Numerical Methods, 3(3), pp. 173 – 180.

[7] Lu, X., Liu, D., 1992, "An interlaminar shear stress continuity theory for both thin and thick composite laminates", Journal of Applied Mechanics, 59(3), pp. 502 – 509.

[8] Di Sciuva, M., 1985, "Development of an anisotropic, multilayered, shear-deformable rectangular plate element", Computers and Structures, 21(4), pp. 789 – 796.

[9] Di Sciuva, M., 1992, “Multilayered anisotropic plate models with continuous interlaminar stresses”, Composite Structures, 22(3), pp. 149 – 167.

[10] Cho, M., Parmenter, R.R., 1993, “Efficient higher order composite plate theory for general lamination configurations”, AIAA Journal, 31(7), pp. 1299 – 1306.

[11] Tessler, A., Di Sciuva, M., Gherlone, M., 2009, “A Refined Zigzag beam Theory for composite and sandwich beams”, Journal of Composite Materials, 43(9), pp. 1051 – 1081.

[12] Tessler, A., Di Sciuva, M., Gherlone, M., 2010, “A consistent refinement of first-order shear-deformation theory for laminated composite and sandwich plates using improved zigzag kinematics”, Journal of Mechanics of Materials and Structures, 5(2), pp. 341 – 367.

[13] Carrera, E., 2003, “Historical review of zig-zag theories for multilayered plates and shells”, Applied Mechanics Review, 56, pp. 287 – 208.

[14] Gherlone, M., 2013, “On the use of zigzag functions in equivalent single layer theories for laminated composite and sandwich beams: a comparative study and some observations on external weak layers”, Journal of Applied Mechanics, 80(6).

[15] Icardi. U., Sola, F., 2016, “Assessment of recent zig-zag theories for laminated and sandwich structures”, Composites Part B: Engineering, 97, pp.26 – 52.

[16] Tessler, A., Di Sciuva, M., Gherlone, M., 2011, “A homogeneous limit methodology and refinements of computationally efficient zigzag theory for homogeneous, laminated composite, and sandwich plates”, Numerical Methods for Partial Differential Equations, 27(1), pp. 208 – 229.

[17] Iurlaro, L., Gherlone, M., Di Sciuva, M., Tessler, A., 2013, “Assessment of the Refined Zigzag Theory for bending, vibration, and buckling of sandwich plates: a comparative study of different theories”, Composite Structures, 106, pp. 777 – 792.

[18] Iurlaro, L., Gherlone, M., Di Sciuva, M., 2014, “Bending and free vibration analysis of functionally graded sandwich plates using the refined zigzag theory”, Journal of Sandwich Structures and Materials, 16, pp. 669 – 699.

[19] Reissner, E., 1984, “On a certain mixed variational theorem and a proposed application”, International Journal for Numerical Methods in Engineering, 20(7), pp. 1366 – 1368.

[20] Murakami, H., 1986, “Laminated composite plate theory with improved in-plane responses”, J Journal of Applied Mechanics, 53(3), pp. 661 – 666.

[21] Toledano, A., Murakami, H., 1987, “A composite plate theory for arbitrary laminate configurations”, Journal of Applied Mechanics, 54(1), pp. 181 – 189.

[22] Wu, Chih-Ping, Li, Hao-Yuan, 2010, “An RMVT-based third-order shear deformation theory of multilayered functionally graded material plates”, Composite Structures, 92(10), pp. 2591 – 2605.

[23] Brischetto, S., Carrera, E., 2010, “Advanced mixed theories for bending analysis of functionally graded plates, “ Computers and Structures, 88(23–24), pp. 1474 - 1483.

[24] Fazzolari, F.A., Banerjee, J.R., 2014, “Axiomatic/asymptotic PVD/RMVT-based shell theories for free vibrations of anisotropic shells using an advanced Ritz formulation and accurate curvature descriptions”, Composite Structures, 108, pp. 91 – 110.

[25] Groh, R.M.J., Weaver, P.M., 2015, “On displacement-based and mixed-variational equivalent single layer theories for modelling highly heterogeneous laminated beams”, International Journal of Solids and Structures, 59(1), pp. 147 – 170.

[26] Vidal, P., Gallimard, L., Polit, O., 2016, “Modeling of composite plates based on Reissner's Mixed Variational Theorem with variables separation”, Composites Part B: Engineering, 86(1), pp. 229 – 242.

[27] Carrera, E., 2001, “Developments, ideas and evaluations based upon Reissner’s mixed variational theorem in the modeling of multilayered plates and shells”, Applied Mechanics Review, 54(4), pp. 301 - 329.

[28] Auricchio, F., Sacco, E., 2003, “Refined first-order shear deformation theory models for composite laminates”, Journal of Applied Mechanics, 70, pp. 381 – 390.

[29] Tessler, A., 2015 “Refined Zigzag Theory for homogeneous, laminated composite, and sandwich beams derived from Reissner’s mixed variational principle”, Meccanica, 50(10), pp. 2621 – 2648.

[30] Groh, R.M.J., Tessler, A., 2017, “Computationally efficient beam elements for accurate stresses in sandwich laminates and laminated composites with delaminations”, Computer Methods in Applied Mechanics and Engineering, 320, pp. 369 – 395.

[31] Iurlaro, L., Gherlone, M., Di Sciuva, M., Tessler, A., 2015, “Refined Zigzag Theory for laminated composite and sandwich plates derived from Reissner’s Mixed Variational Theorem”, Composite Structures, 133, pp. 809 – 817.

[32] Gherlone, M., 2018, “A class of plate finite elements based on the mixed Refined Zigzag Theory for the analysis of multilayered composite and sandwich plates”,

XXVIII International Workshop on Computational Mechanics of Materials, Glasgow, September 10 – 12, 2018.

[33] Versino, D., Mattone, M., Gherlone, M., Tessler, A., and Di Sciuva, M., 2013, "An efficient, C^0 triangular elements based on the Refined Zigzag Theory for multilayered composite and sandwich plates", Composites Part B: Engineering, 44(1), pp. 218 – 230.

[34] Tessler, A., Dong., S.B., 1981, "On a hierarchy of conforming Timoshenko beam elements", Computers and Structures, 14(3-4), pp. 335 – 344.

[35] Tessler, A., Hughes, T.J.R., 1983, "An improved treatment of transverse shear in the Mindlin-type four-node quadrilateral element", Computer Methods in Applied Mechanics and Engineering, 39, pp. 311 – 355.

[36] Tessler, A., Hughes, T.J.R., 1985, "A three-node Mindlin plate element with improved transverse shear", Computer Methods in Applied Mechanics and Engineering, 50(1), pp. 71 – 101.

[37] Zienkiewicz, O.C., Taylor., R.L., 2005, "The finite element method for solid and structural mechanics", Elsevier, 6th edition.

[38] Pagano, N.J., 1969, "Exact solutions for composite laminates in cylindrical bending", Journal of Composite Materials, 3, pp. 398 – 411.

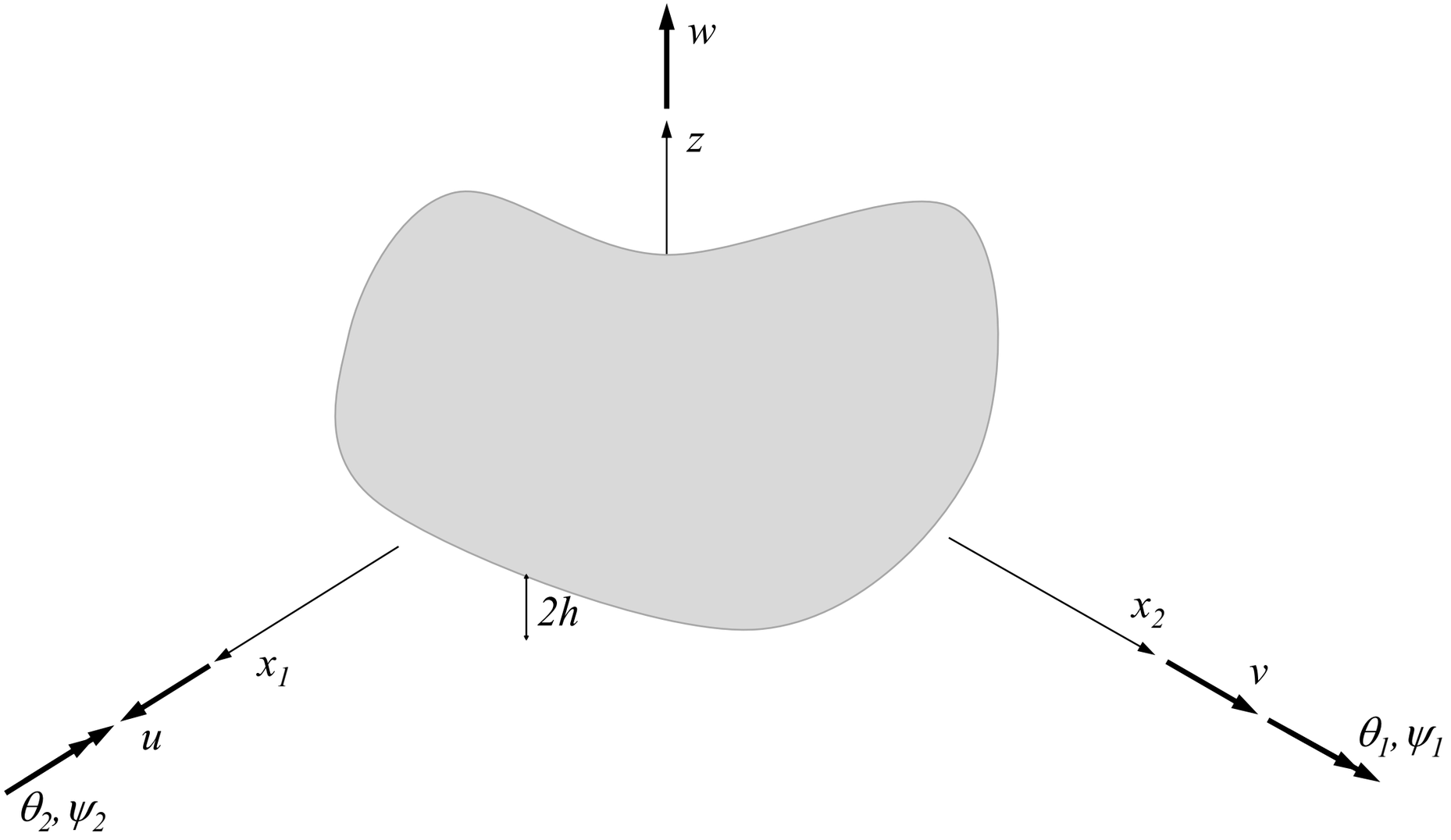
w
z
2h
x1
u
θ2, ψ2
x2
v
θ1, ψ1

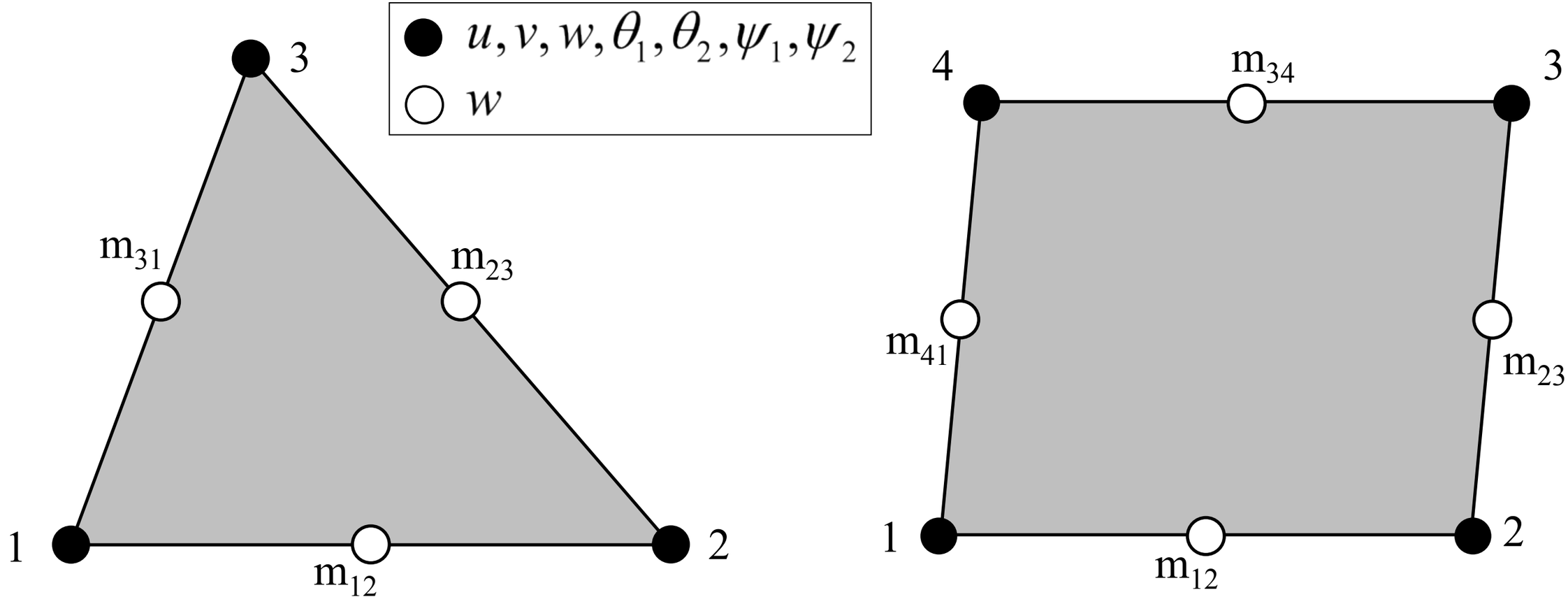
$u, v, w, \theta_1, \theta_2, \psi_1, \psi_2$
w
1
2
3
m_{12}
m_{23}
m_{31}
1
2
3
4
m_{12}
m_{23}
m_{34}
m_{41}

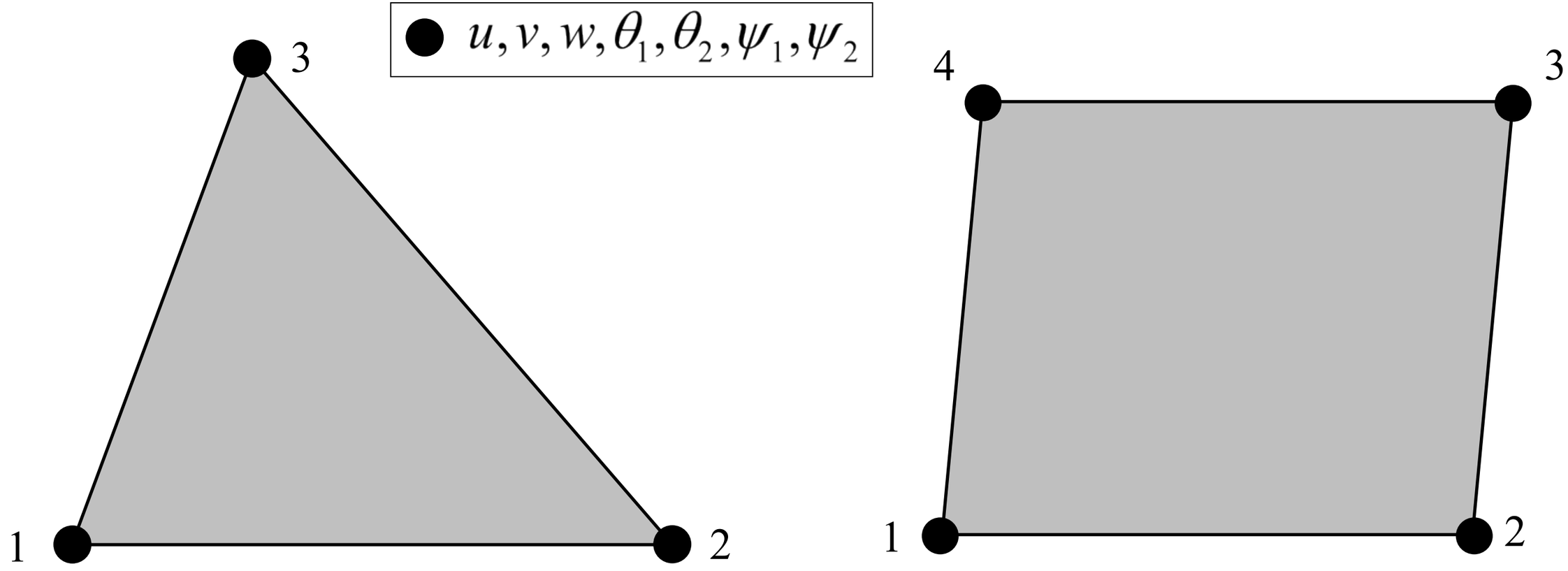
$u, v, w, \theta_1, \theta_2, \psi_1, \psi_2$
3
1
2
4
3
1
2

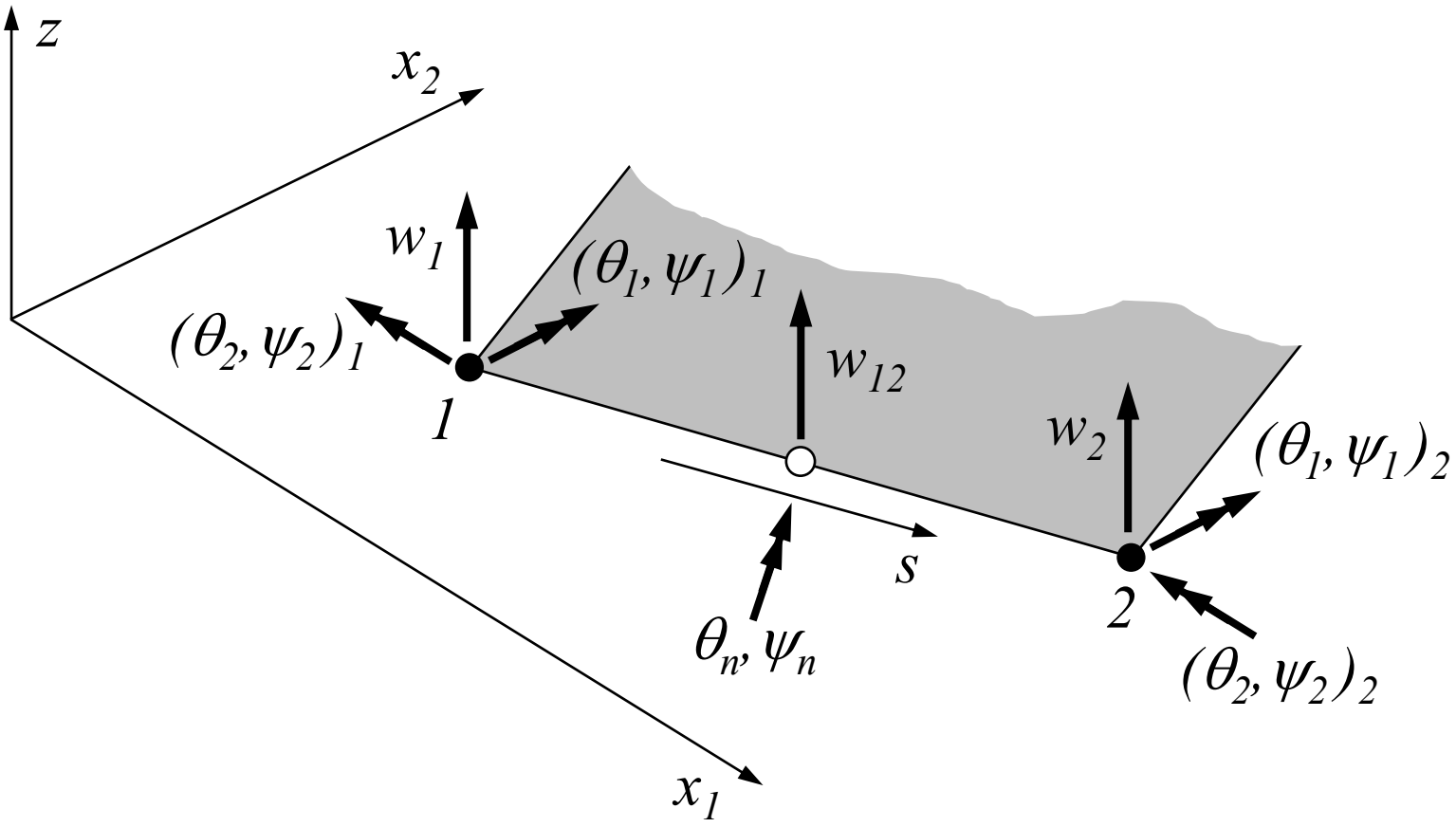
z
x_2
w_1
$(\theta_1, \psi_1)_1$
$(\theta_2, \psi_2)_1$
1
w_{12}
w_2
$(\theta_1, \psi_1)_2$
s
2
θ_n, ψ_n
$(\theta_2, \psi_2)_2$
x_1

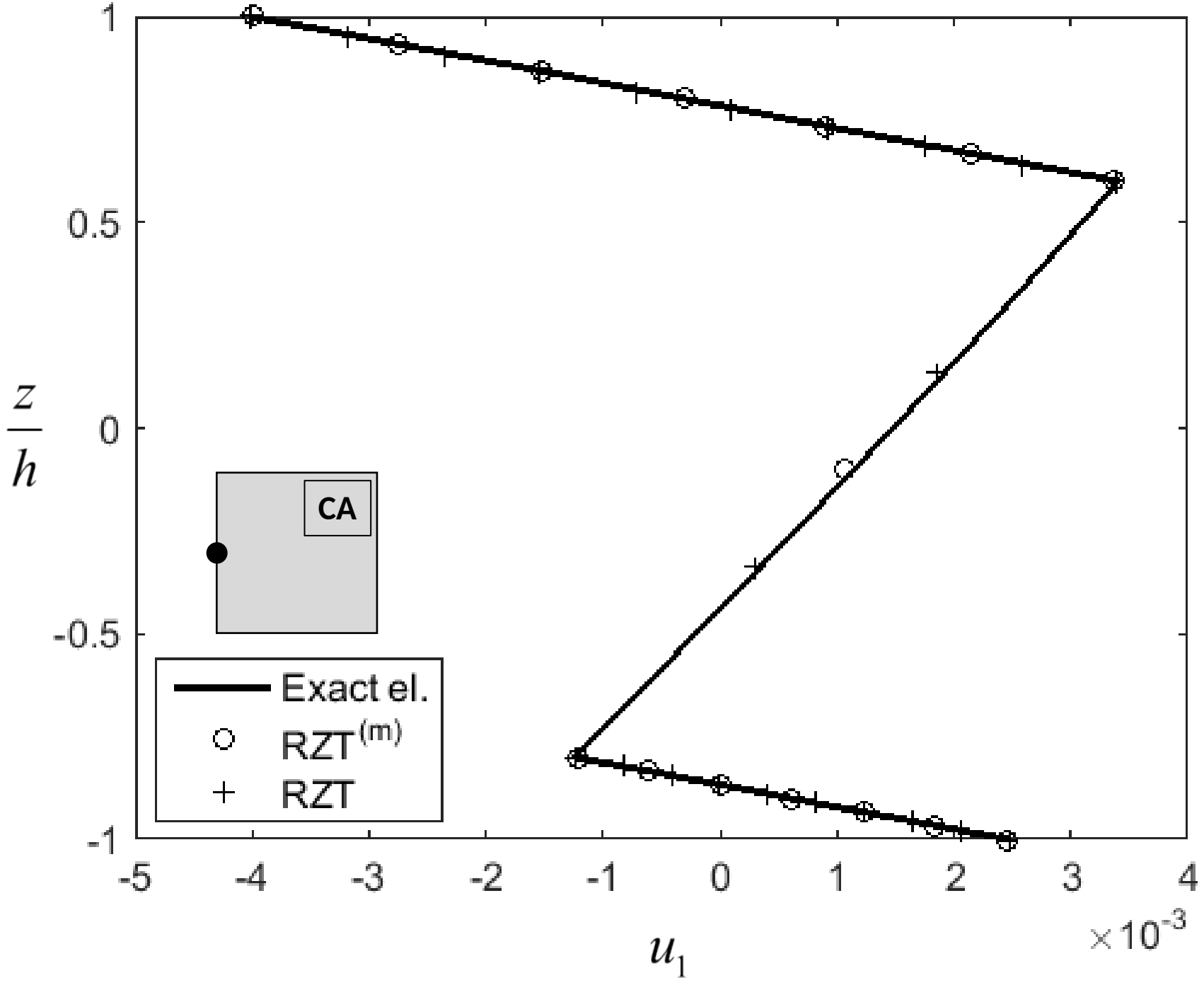
1
0.5
0
-0.5
-1
$\frac{z}{h}$
-5
-4
-3
-2
-1
0
1
2
3
4
$\times 10^{-3}$
u_1
CA
Exact el.
RZT$^{(m)}$
RZT

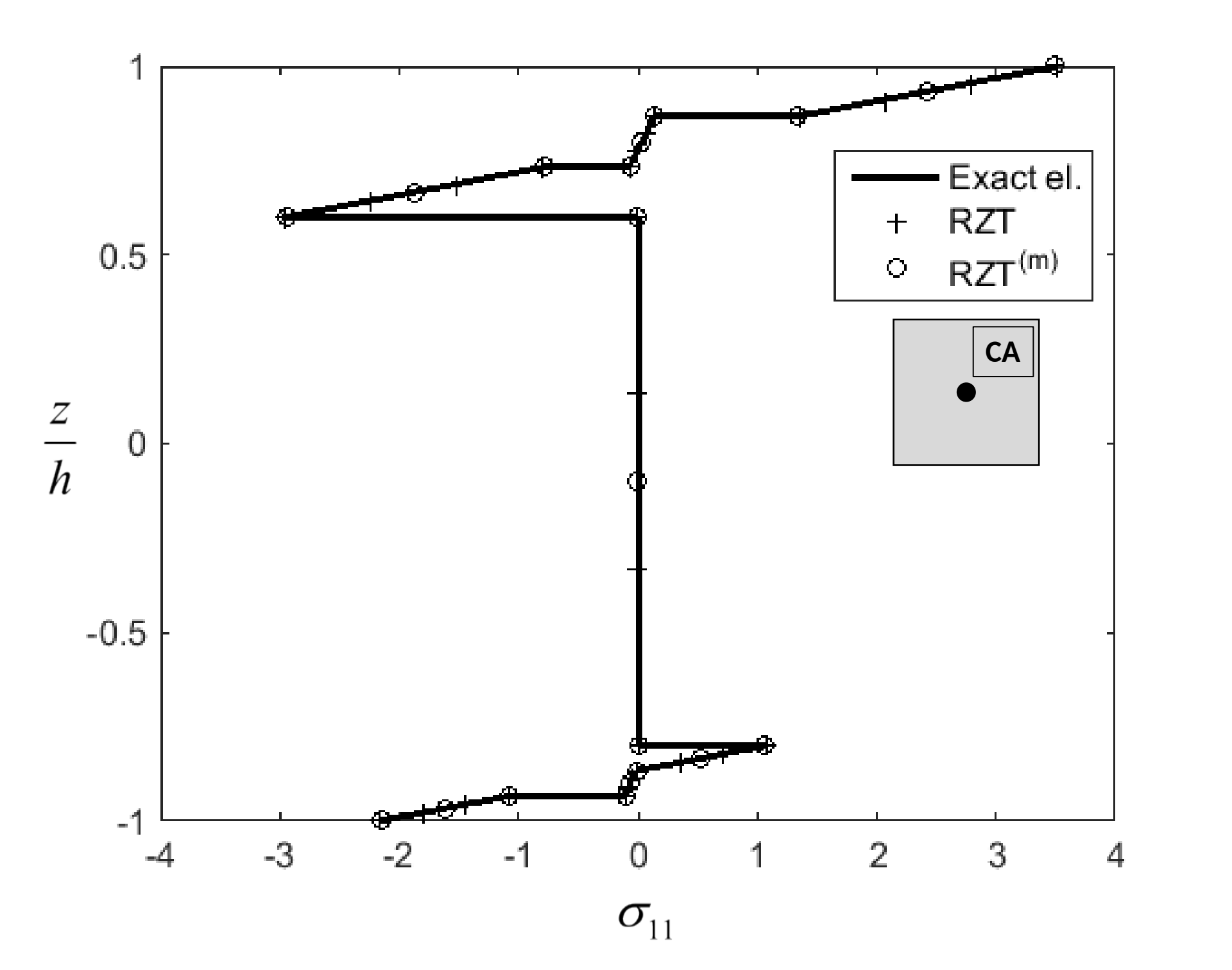
1
0.5
0
-0.5
-1
-4
-3
-2
-1
0
1
2
3
4
z/h
σ11
Exact el.
RZT
RZT(m)
CA

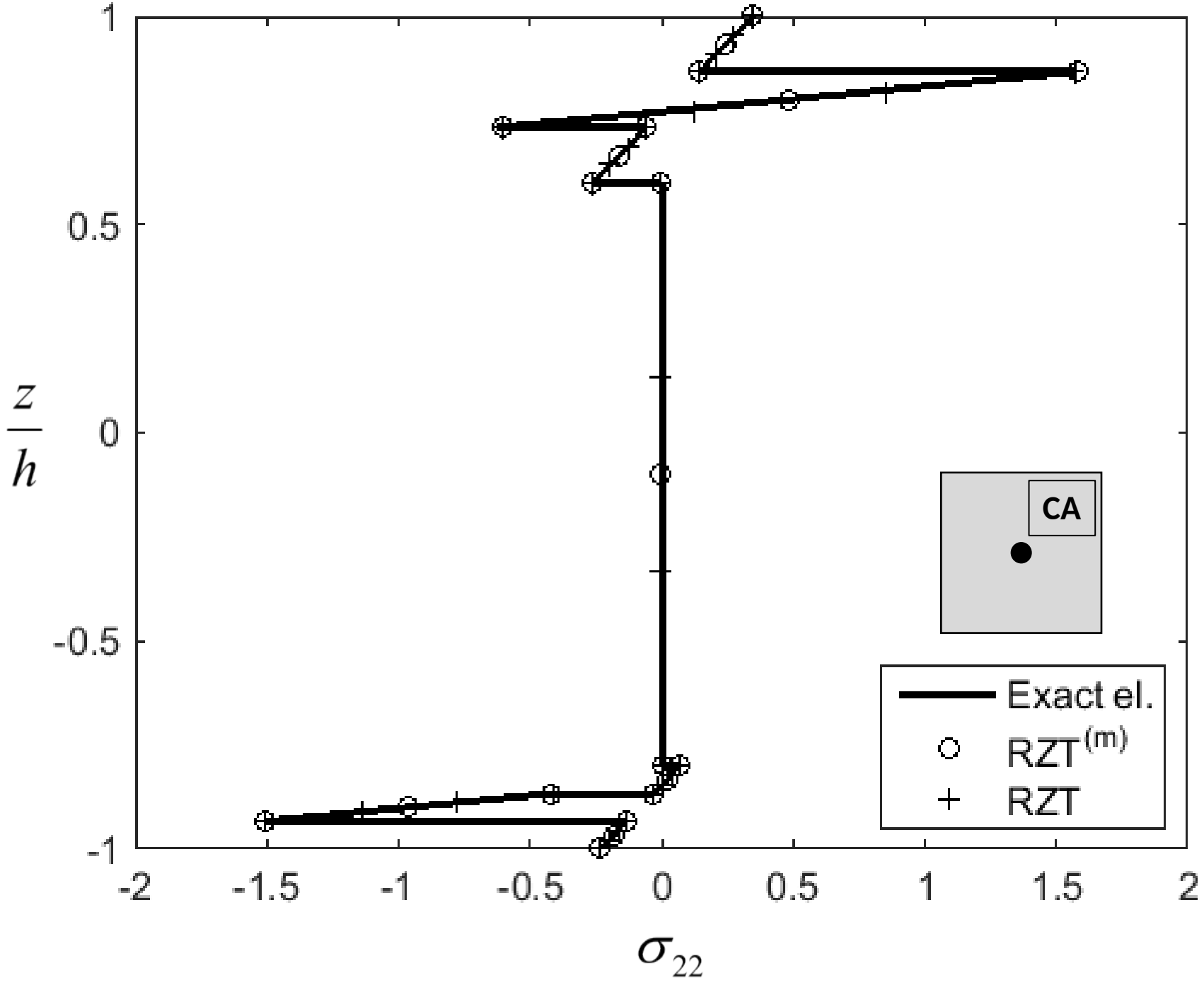
1
0.5
0
-0.5
-1
-2
-1.5
-1
-0.5
0
0.5
1
1.5
2
z/h
σ22
CA
Exact el.
RZT(m)
RZT

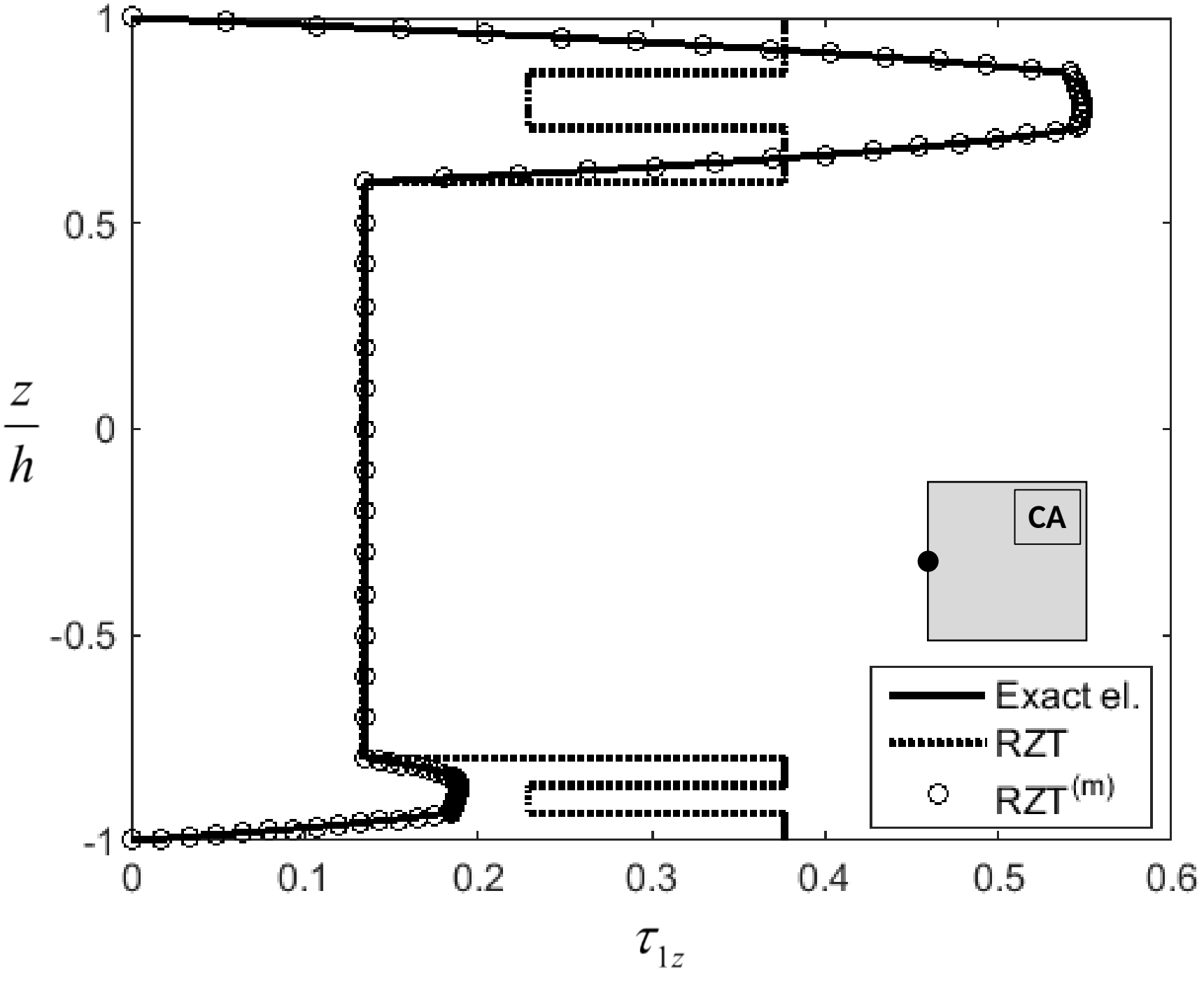
1
0.5
0
-0.5
-1
0
0.1
0.2
0.3
0.4
0.5
0.6
$\frac{z}{h}$
τ_{1z}
CA
Exact el.
RZT
RZT$^{(m)}$

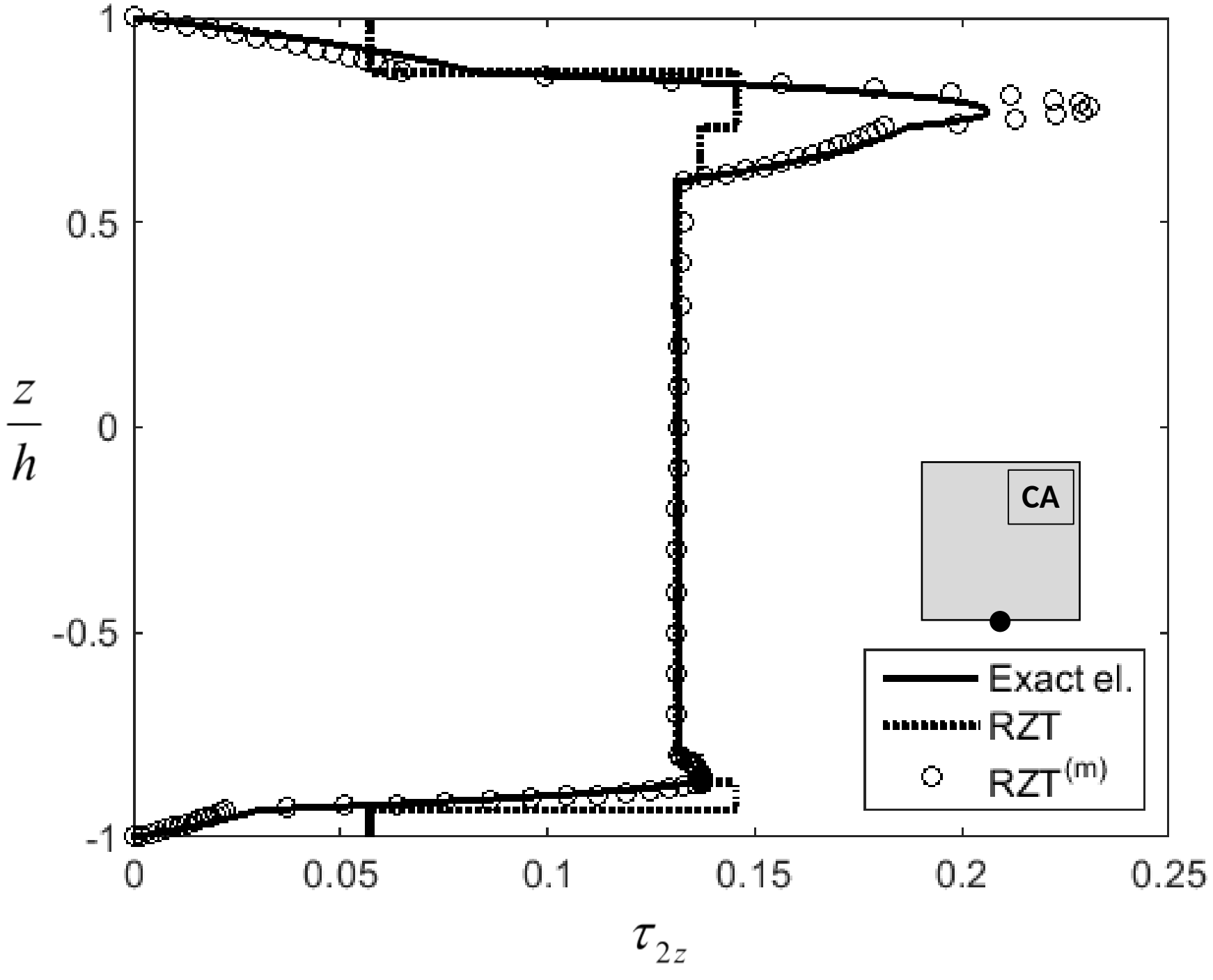
1
0.5
0
-0.5
-1
0
0.05
0.1
0.15
0.2
0.25
$\frac{z}{h}$
τ_{2z}
CA
Exact el.
RZT
RZT$^{(m)}$

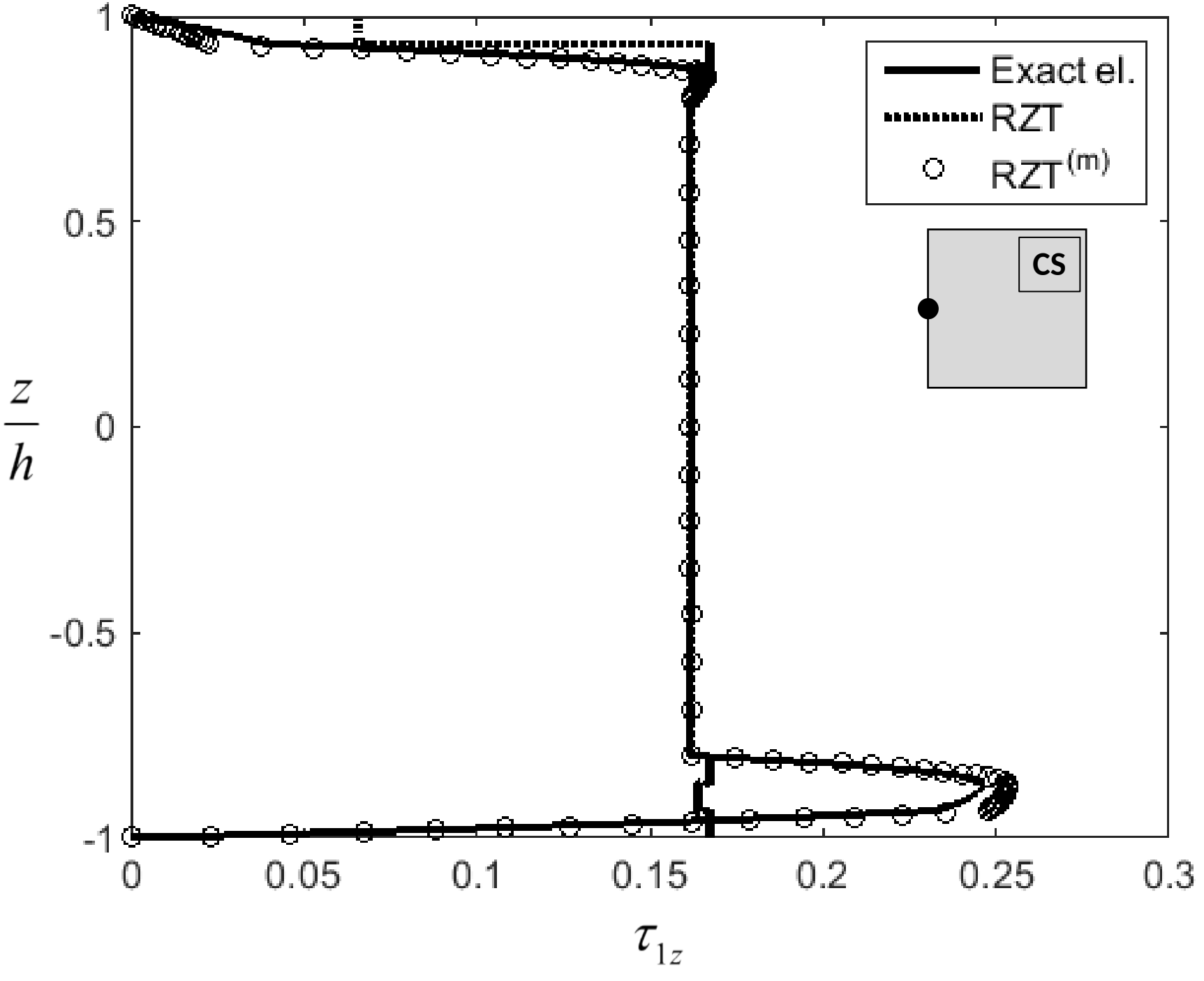
Exact el.
RZT
RZT(m)
CS
z/h
1
0.5
0
-0.5
-1
0
0.05
0.1
0.15
0.2
0.25
0.3
τ1z

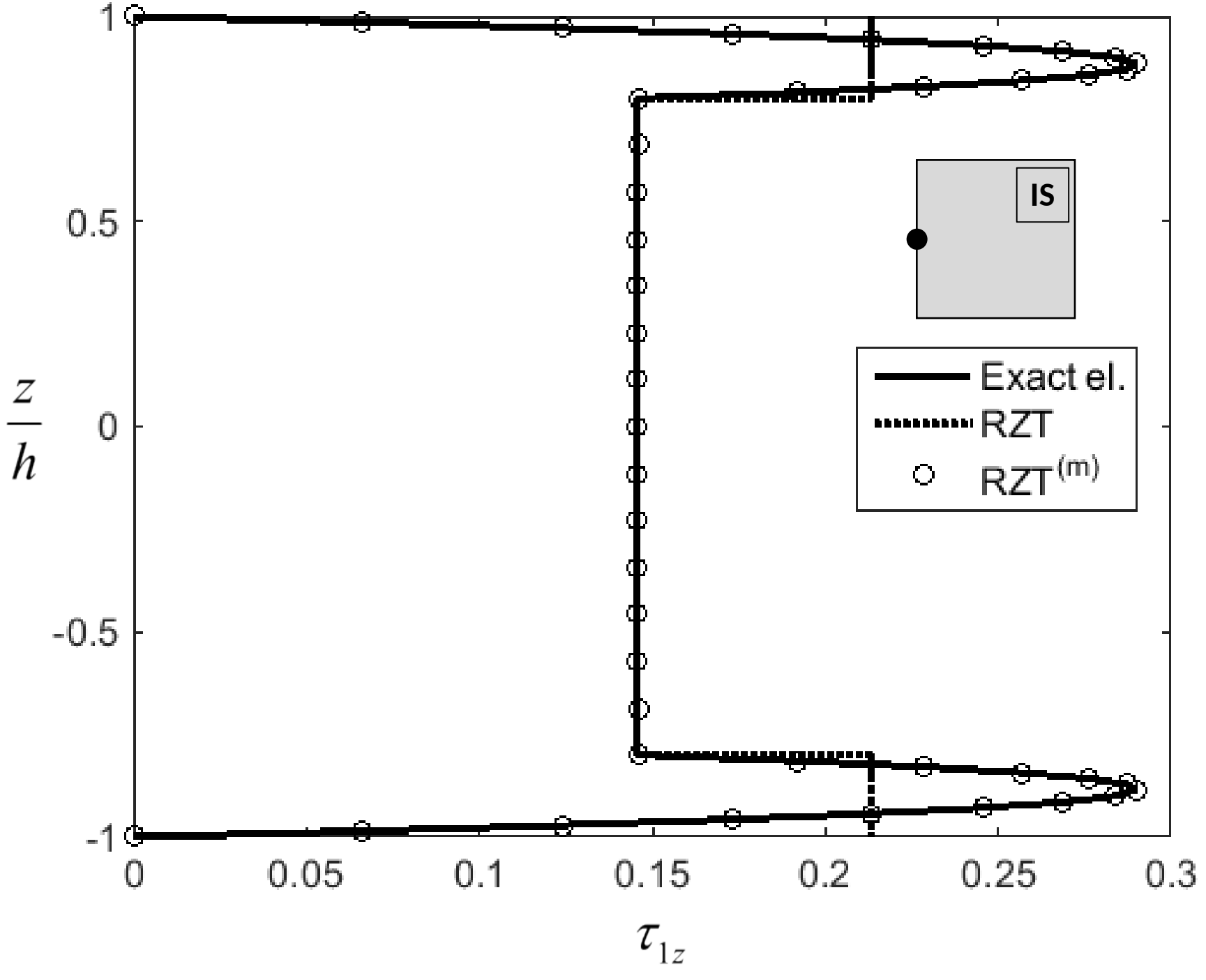
1
0.5
0
-0.5
-1
0
0.05
0.1
0.15
0.2
0.25
0.3
$\frac{z}{h}$
τ_{1z}
IS
Exact el.
RZT
RZT(m)

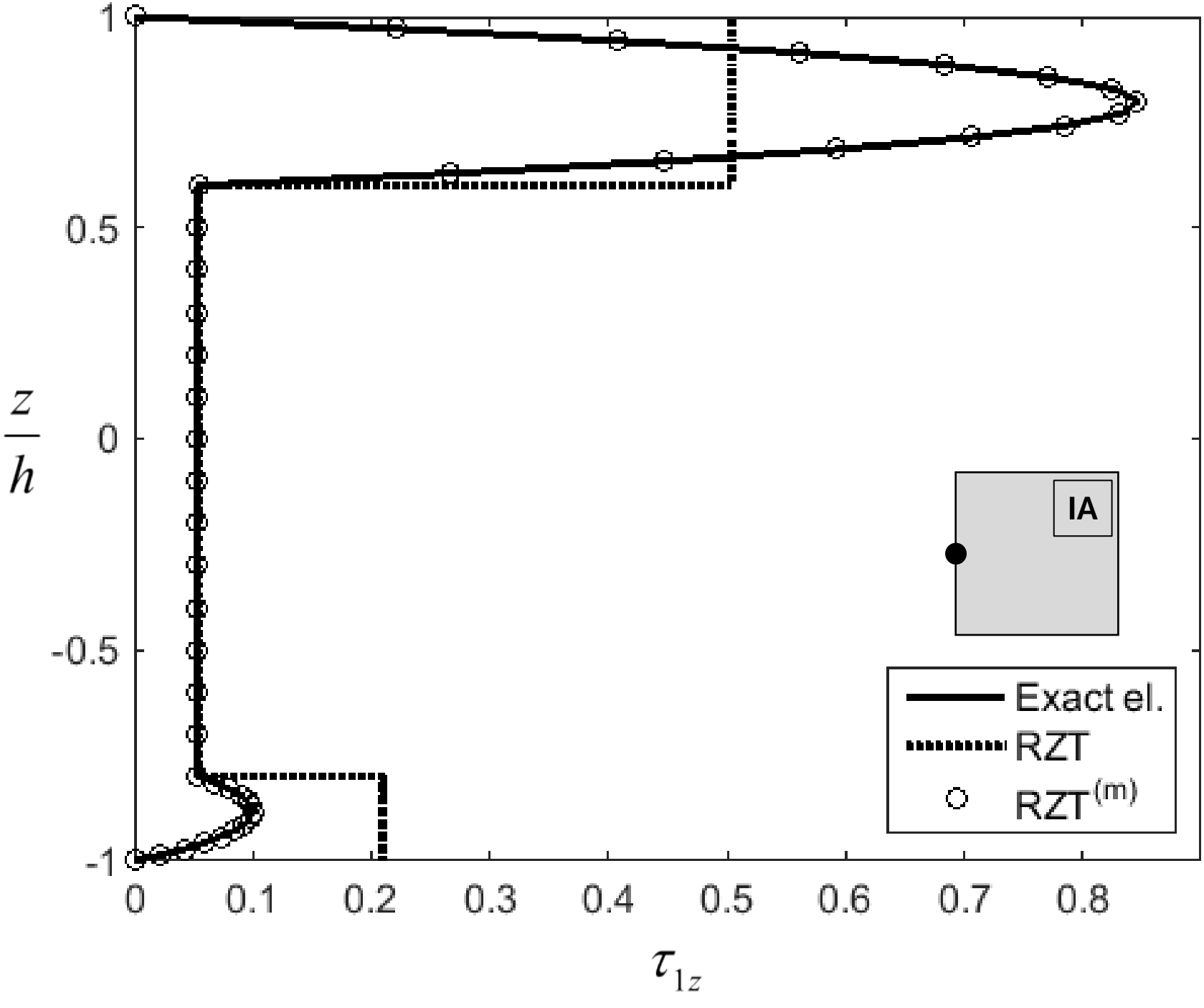
1
0.5
0
-0.5
-1
$\frac{z}{h}$
0
0.1
0.2
0.3
0.4
0.5
0.6
0.7
0.8
τ_{1z}
IA
Exact el.
RZT
RZT$^{(m)}$

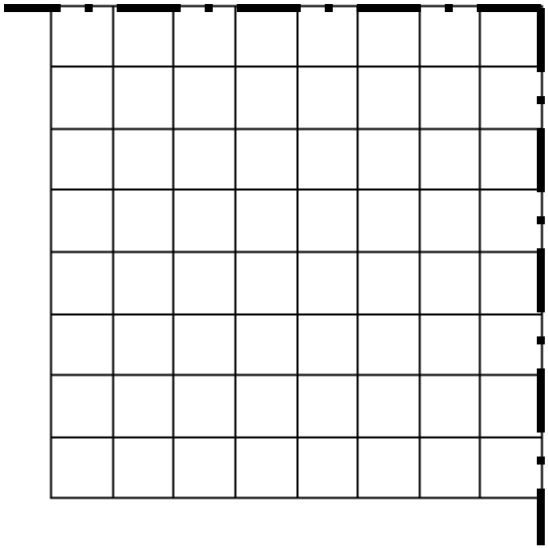

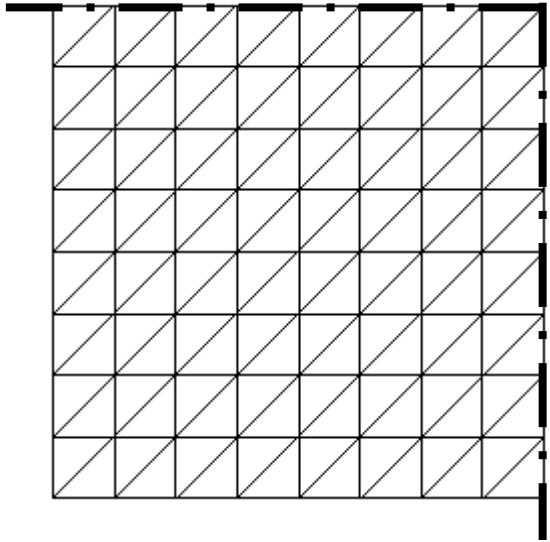

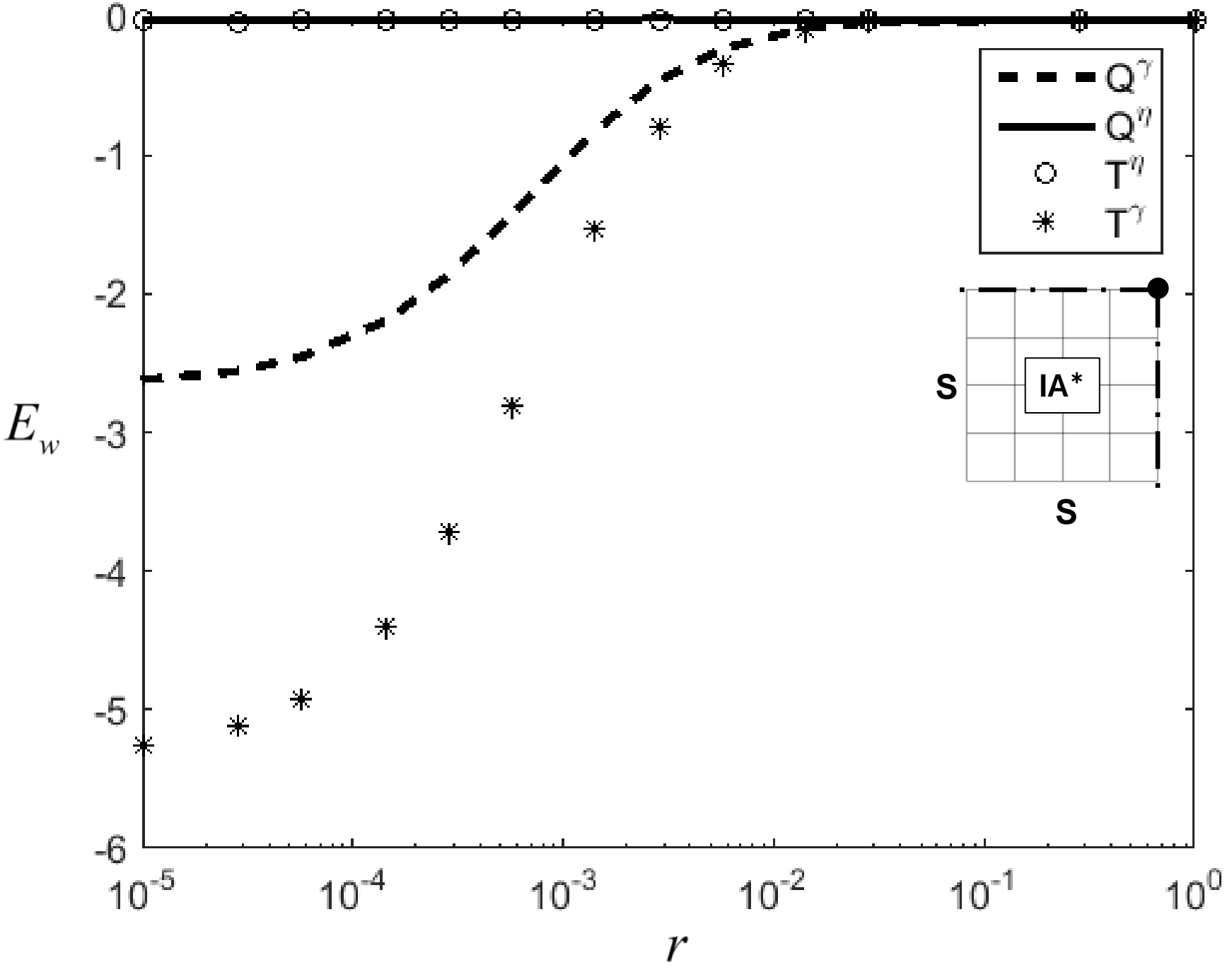
0
-1
-2
-3
-4
-5
-6
E_w
10^{-5}
10^{-4}
10^{-3}
10^{-2}
10^{-1}
10^{0}
r
Q^{γ}
Q^{η}
T^{η}
T^{γ}
S
IA*
S

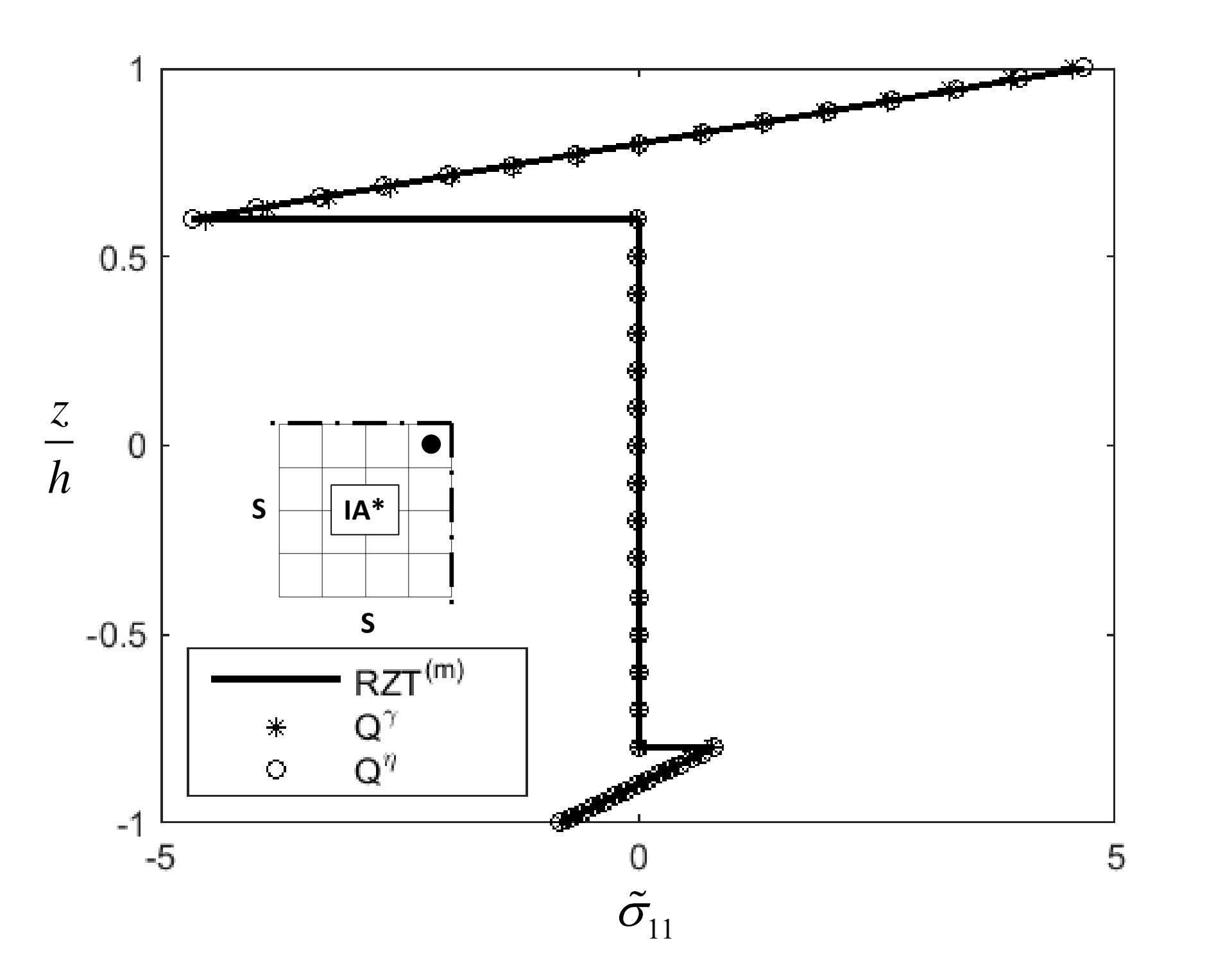
1
0.5
0
-0.5
-1
-5
0
5
$\frac{z}{h}$
$\tilde{\sigma}_{11}$
S
IA*
S
RZT(m)
Qγ
Qη

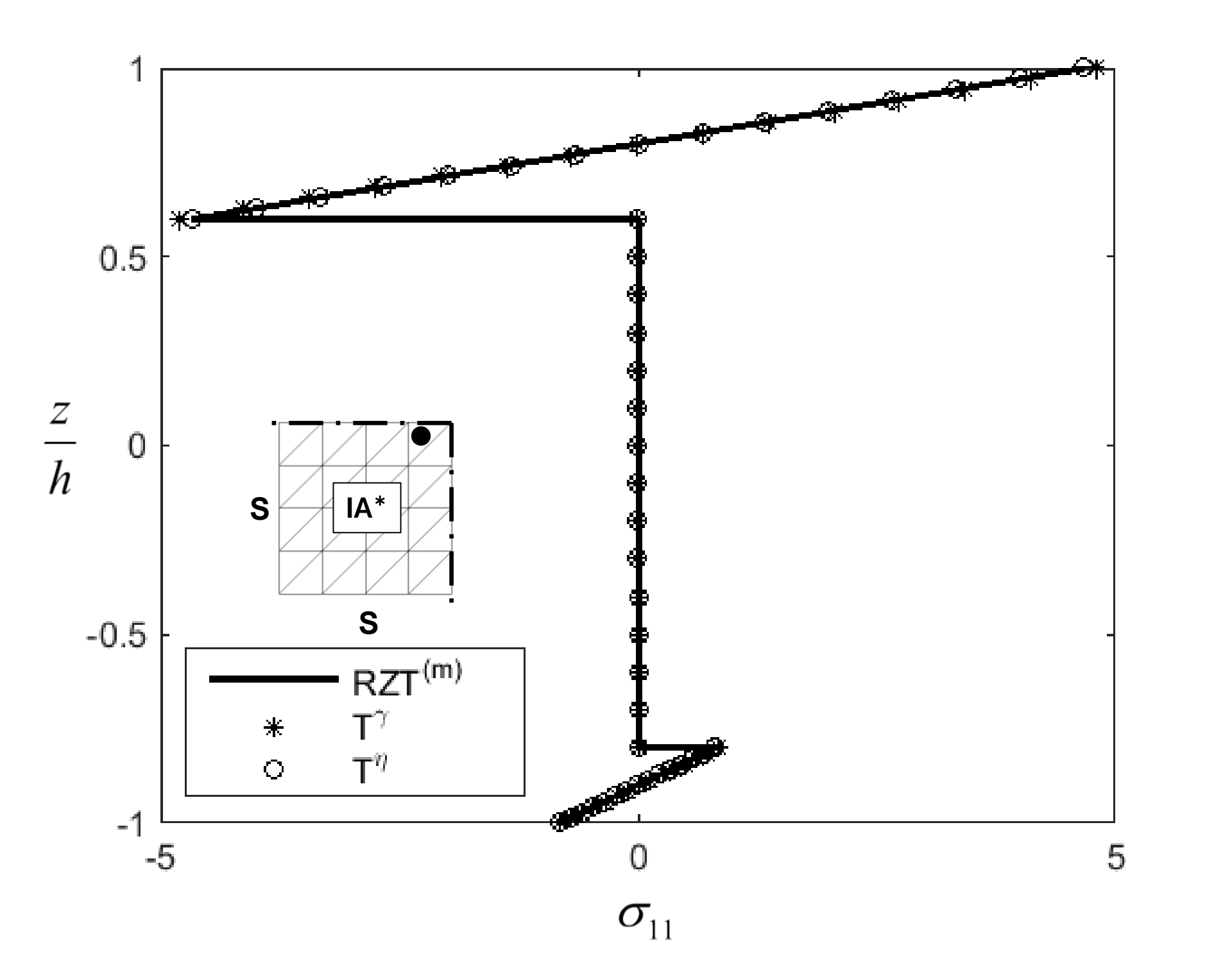
1
0.5
0
-0.5
-1
-5
0
5
$\frac{z}{h}$
σ_{11}
S
IA*
S
RZT(m)
T$^{\gamma}$
T$^{\eta}$

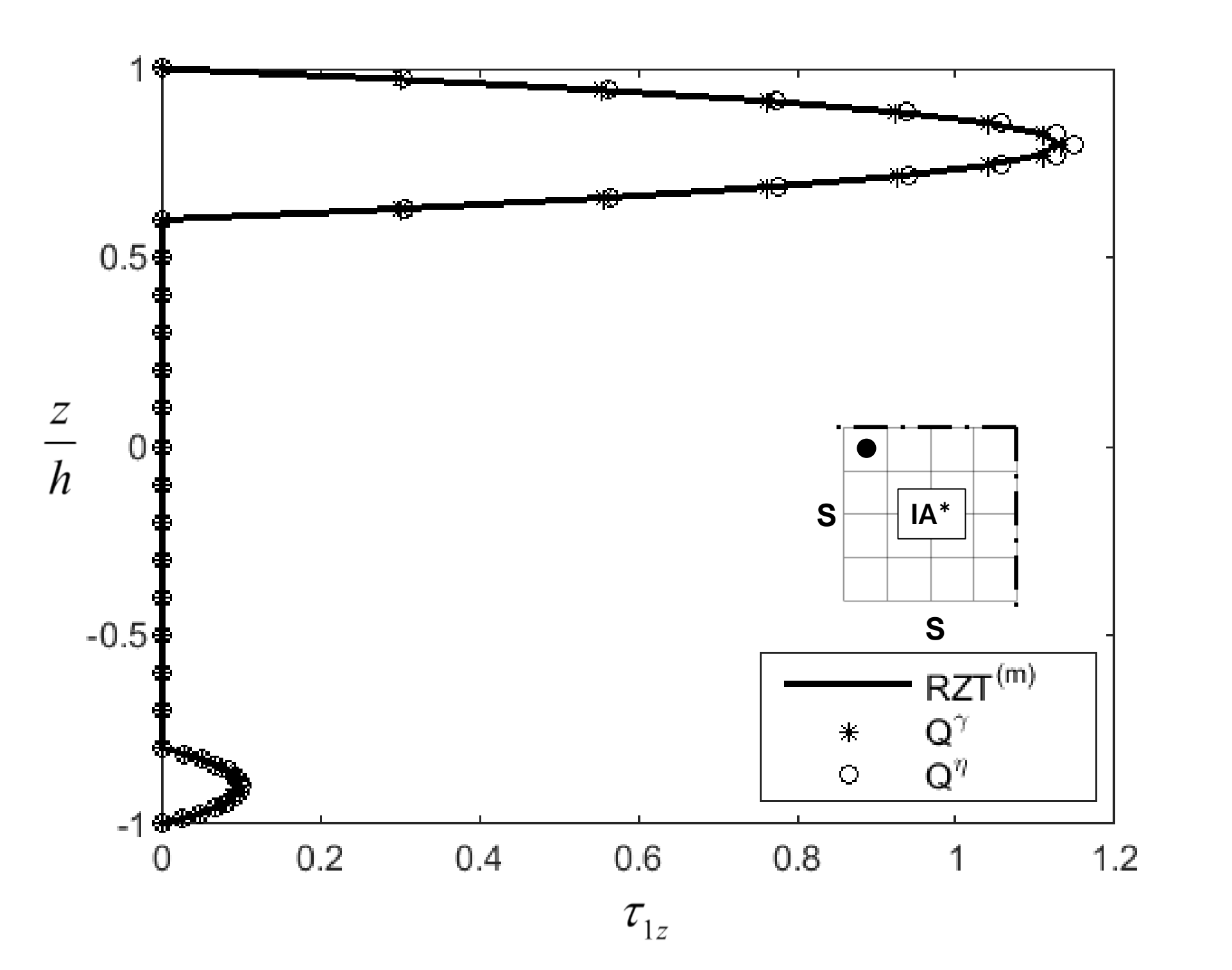
1
0.5
0
-0.5
-1
z/h
0
0.2
0.4
0.6
0.8
1
1.2
τ1z
S
IA*
S
RZT(m)
Qγ
Qη

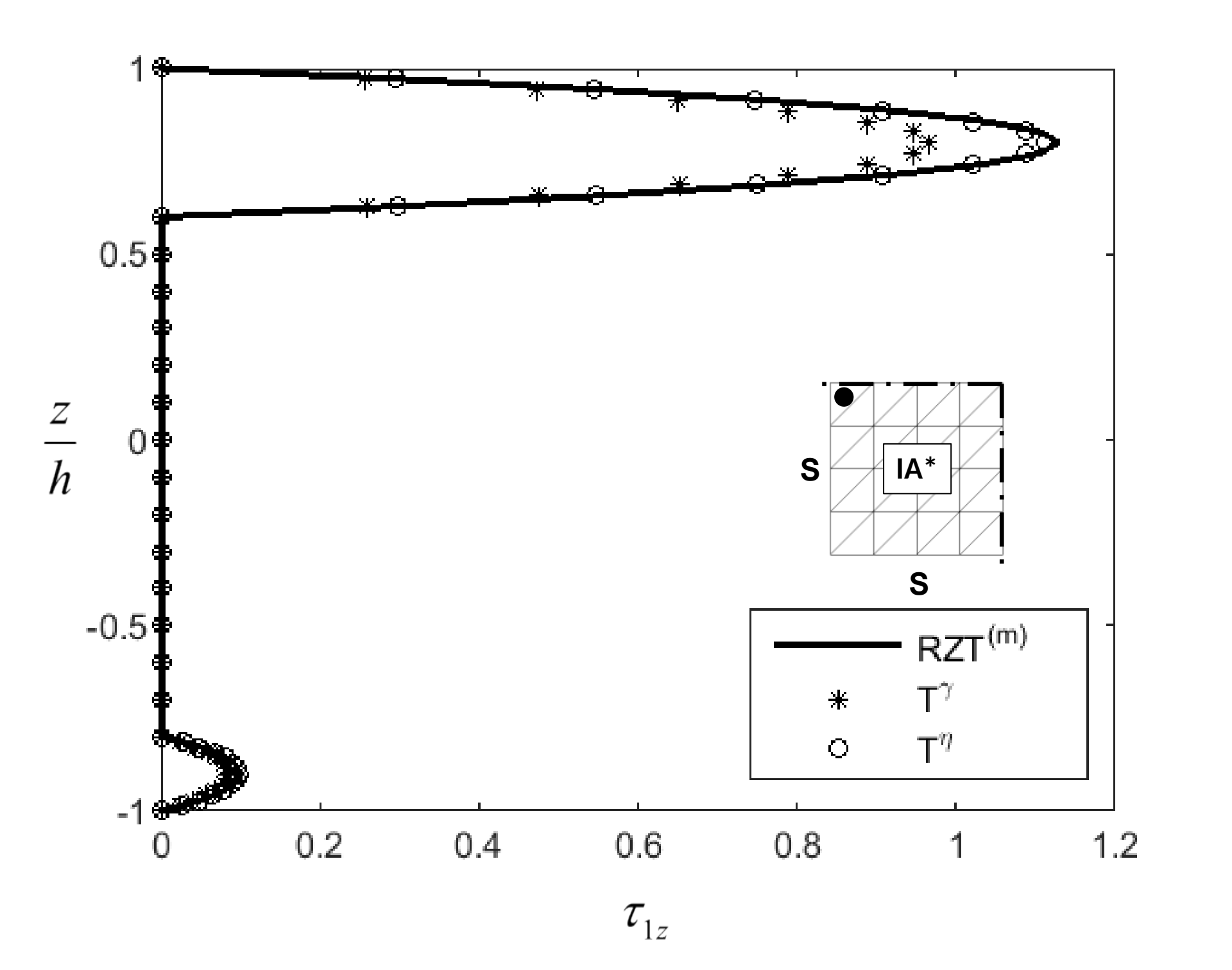
1
0.5
0
-0.5
-1
0
0.2
0.4
0.6
0.8
1
1.2
$\frac{z}{h}$
τ_{1z}
S
IA*
S
RZT(m)
T$^{\gamma}$
T$^{\eta}$

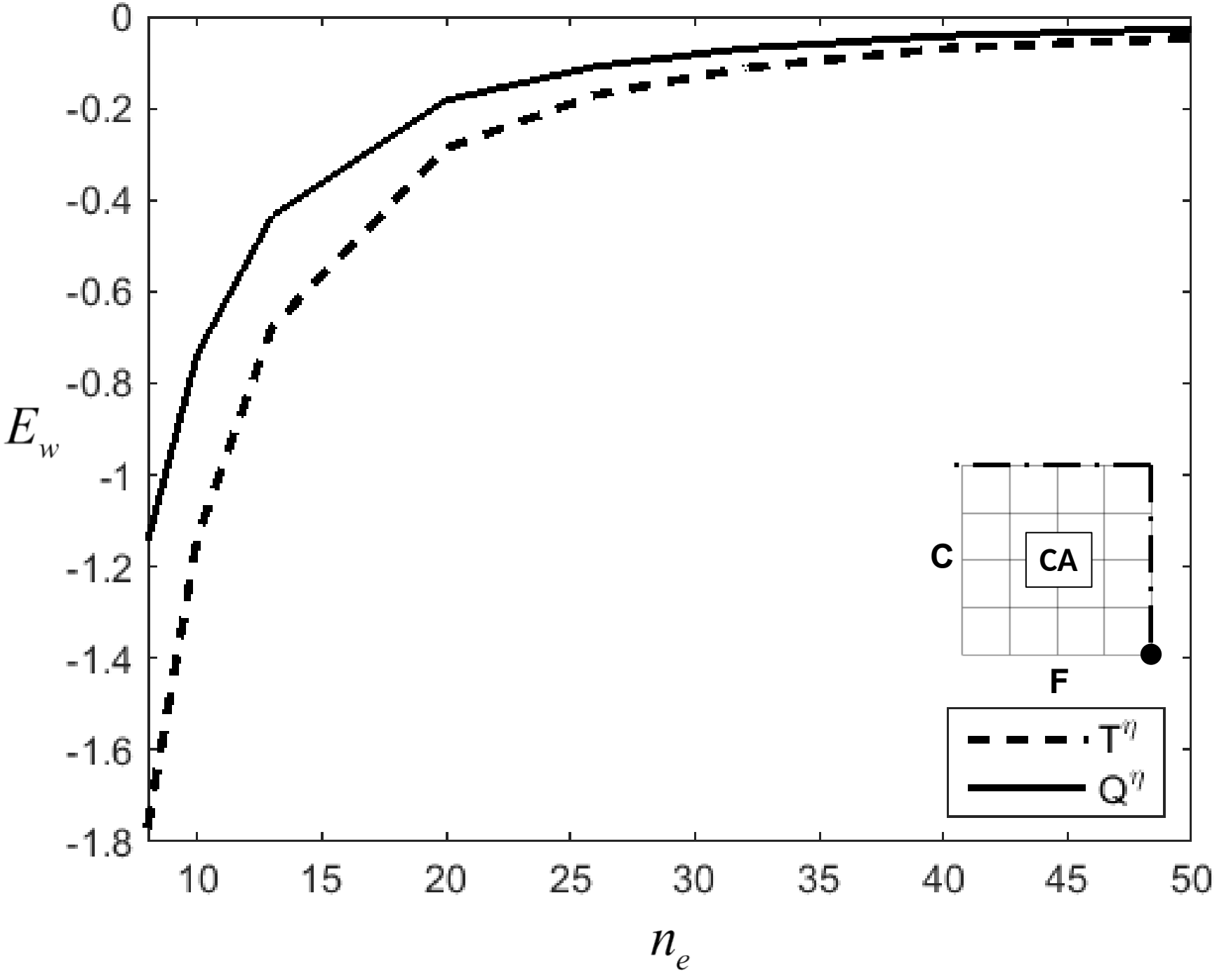
0
-0.2
-0.4
-0.6
-0.8
-1
-1.2
-1.4
-1.6
-1.8
E_w
10
15
20
25
30
35
40
45
50
n_e
C
CA
F
T^{η}
Q^{η}

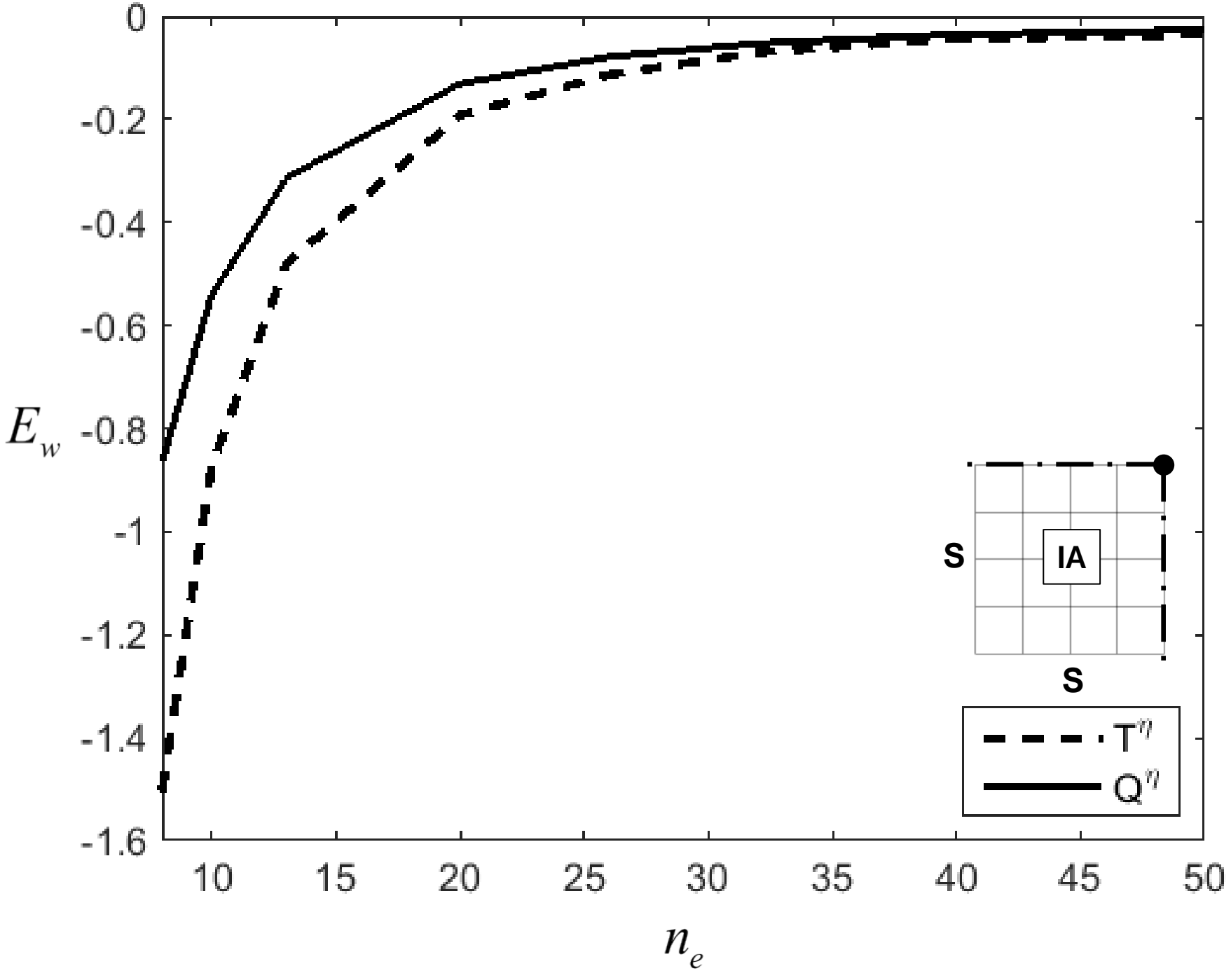
0
-0.2
-0.4
-0.6
-0.8
-1
-1.2
-1.4
-1.6
E_w
10
15
20
25
30
35
40
45
50
n_e
S
IA
S
T^{η}
Q^{η}

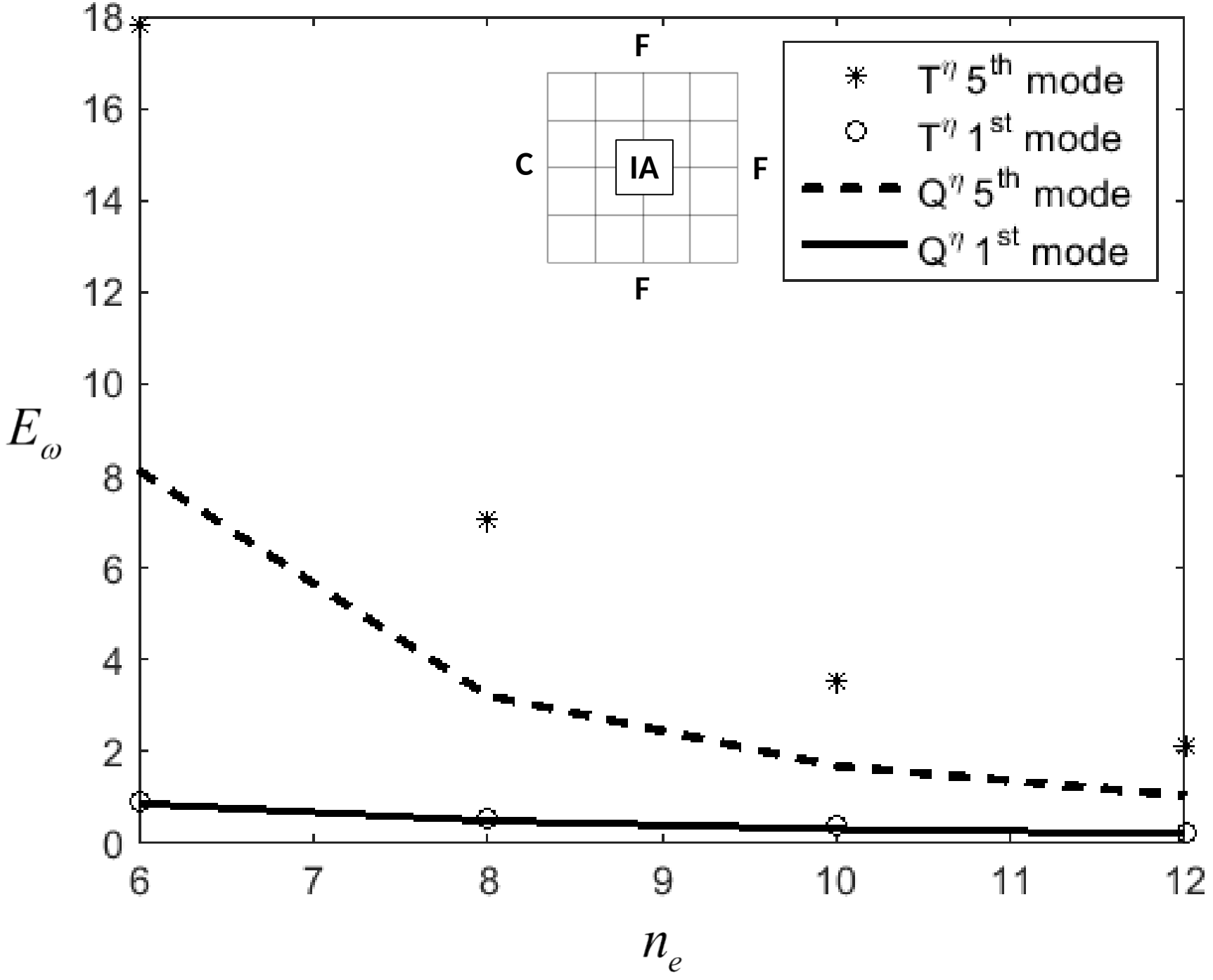
18
16
14
12
10
8
6
4
2
0
6
7
8
9
10
11
12
E_ω
n_e
F
C
IA
F
F
T$^\eta$ 5th mode
T$^\eta$ 1st mode
Q$^\eta$ 5th mode
Q$^\eta$ 1st mode

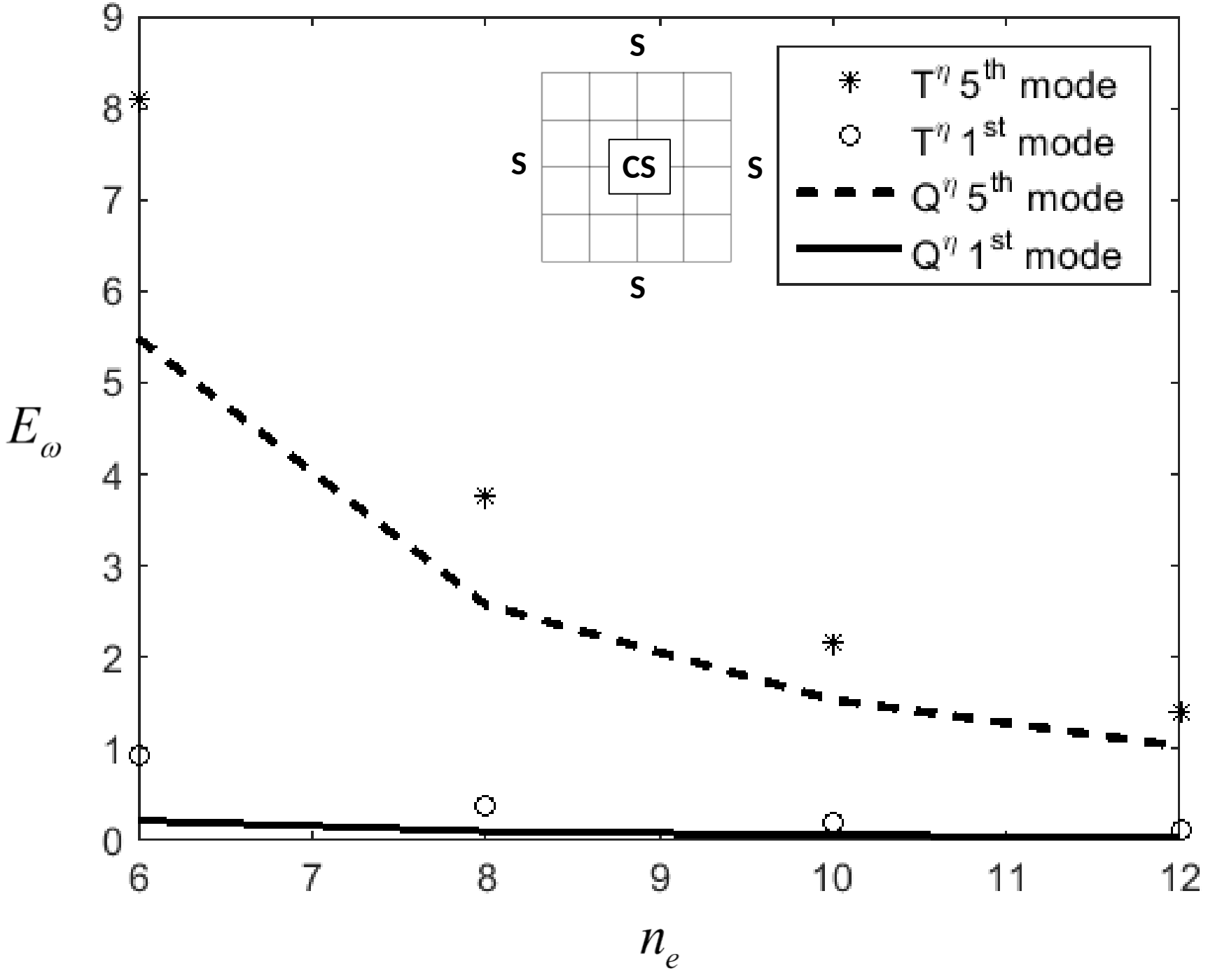
S
S
CS
S
S
T^η 5th mode
T^η 1st mode
Q^η 5th mode
Q^η 1st mode
E_ω
n_e
0
1
2
3
4
5
6
7
8
9
6
7
8
9
10
11
12

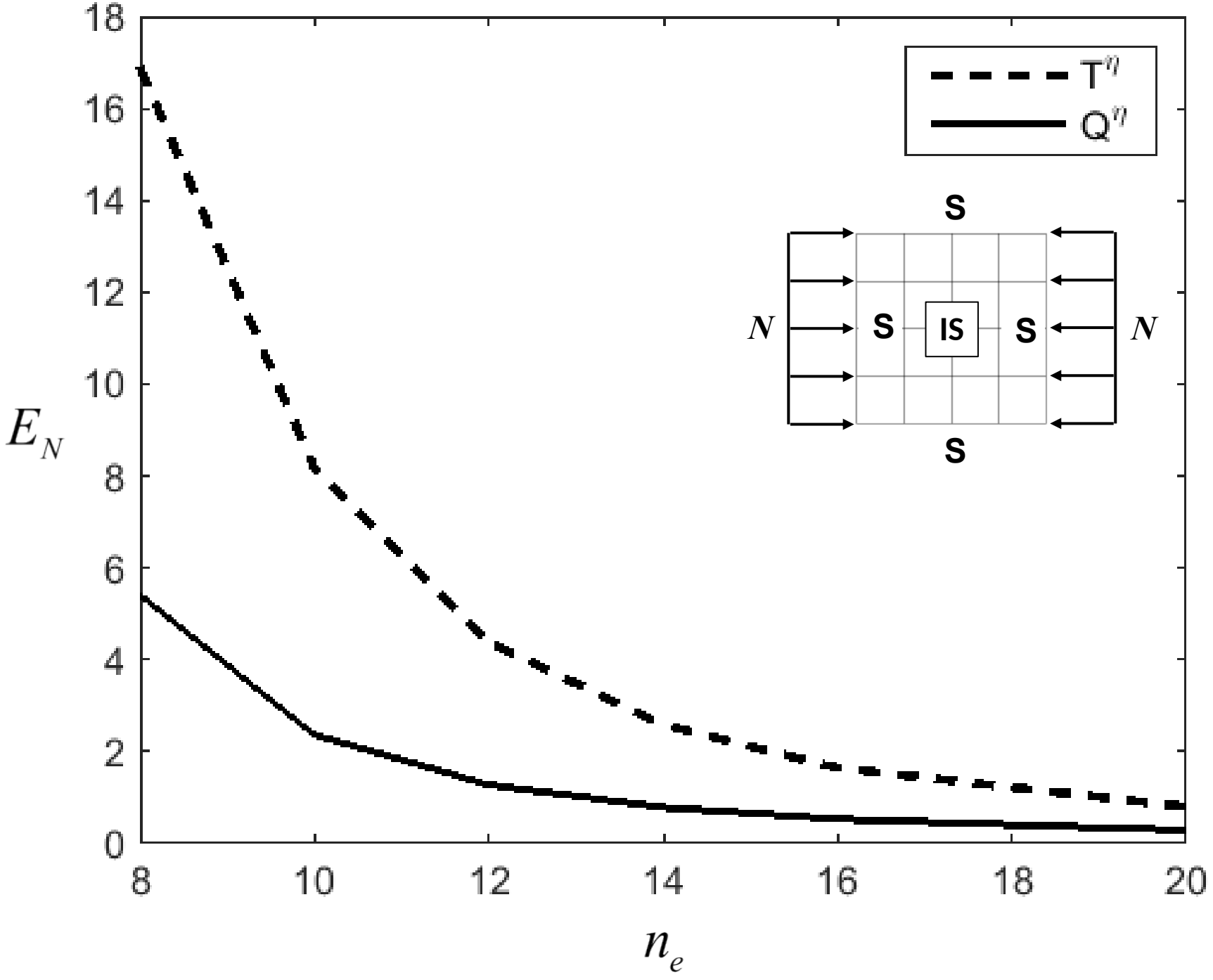
18
16
14
12
10
8
6
4
2
0
8
10
12
14
16
18
20
E_N
n_e
T^η
Q^η
S
N
S
IS
S
N
S

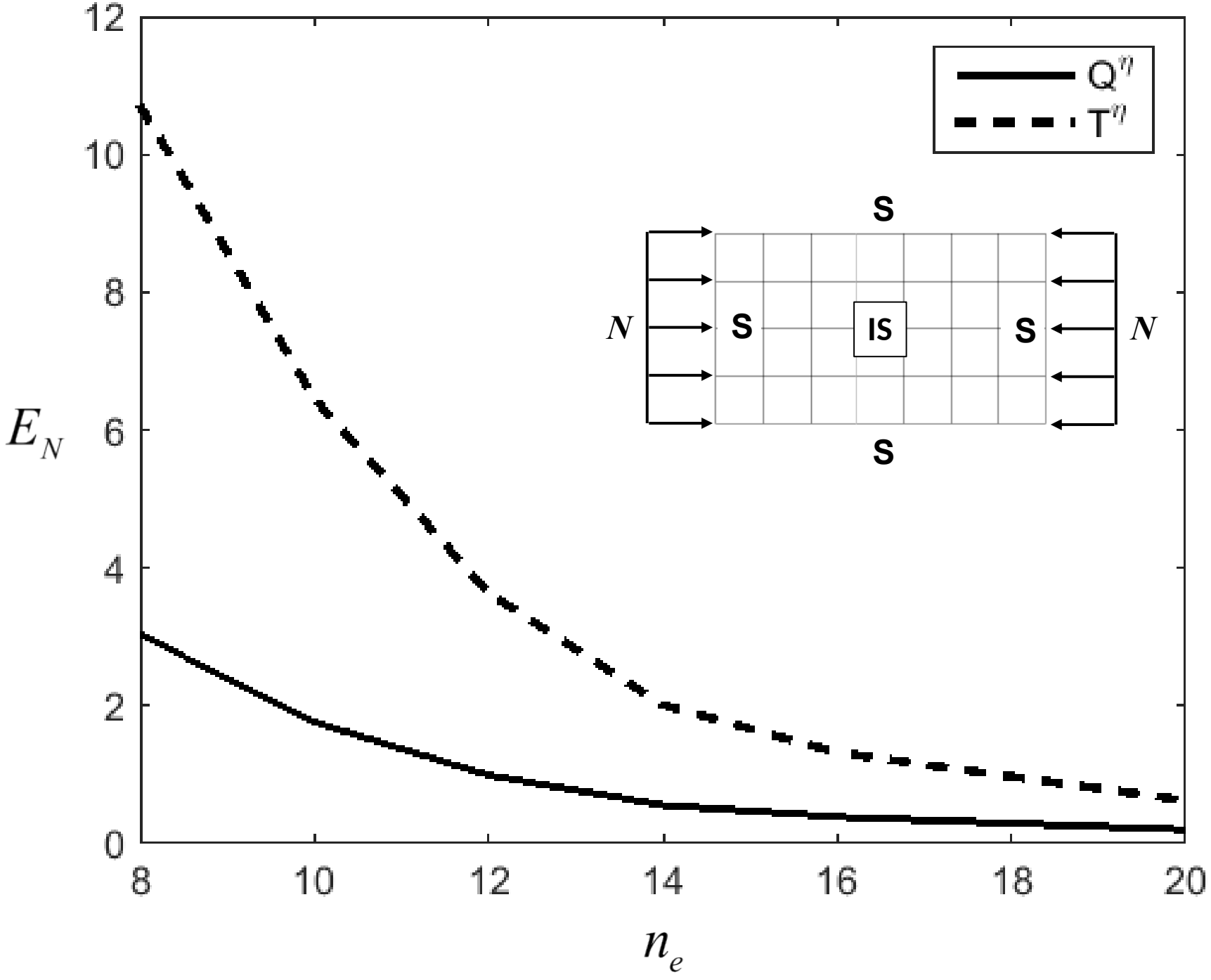
12
10
8
6
4
2
0
8
10
12
14
16
18
20
E_N
n_e
Q^η
T^η
S
N
S
IS
S
N
S